ARTICLES

but the changes were less severe (data not shown). Also, transgenic mice that expressed LAMR1-TP1 in both cardiac chambers showed predominant right ventricular degeneration. It seems possible that the threshold for cardiomyocyte damage is higher in the left ventricle than in the right ventricle. This implies that a higher level of *Lamr1-tp1* expression could cause left ventricular degeneration. Often in human ARVD, a part of the left ventricle is involved. Although both ARVD2 and Naxos disease show a right ventricle–specific phenotype in humans, the genes responsible are equally expressed in both cardiac chambers[6,23]; the mechanism of right ventricular susceptibility is still unknown. The most likely explanation is that specific genes that determine the susceptibility to cell damage exist in either ventricle. Left ventricular cardiomyocytes are under high stress because of the high pressure in this ventricle, and more cytoprotective genes may be induced as a result. In fact, microarray analysis comparing right ventricle and left ventricle shows higher expression in the left ventricle of genes belonging to the category of cell and organism defense[24]. Dominant degeneration of the outer right ventricular wall in ARVD also supports this concept because the inner free wall is under more mechanical stress and expresses more defensive genes, such as heat shock proteins. This mechanism might lead to left ventricle protection in ARVD. Alternatively, right ventricle–specific genes may be involved in the susceptibility of the right ventricle. Mice lacking the right ventricle–specific gene actinin-associated LIM-domain protein show some ARVD-like features[25], even though the histological characteristics are considerably different from those of human ARVD.

We found that one of the heterochromatin complex proteins, HP1-α, showed specific binding to LAMR1-TP1. HP1-α is a key component of condensed DNA and is involved in gene silencing by interaction with methylated histone H3. Mobility of HP1-α has been reported in various cells[18,26]. The stochastic competition between such factors as LAMR1-TP1 and HP1-α may determine the fate of the heterochromatin plasticity that is involved in regulating the fate of cells. Class II histone deacetylase acts as a signal-responsive suppressor of the transcriptional events governing cardiac hypertrophy and heart failure[27]. HP1 can link with class II histone deacetylase[28] and thus may modify cardiac cell metabolism. Accordingly, we conclude that LAMR1-TP1 was translated from an active retroposon in ARVD mice and then interacted with HP1-α, leading to the early death of cardiomyocytes.

Genomic databases indicate that there are up to 40 and 32 *Lamr1* retroposons in humans and mice, respectively. It has also been suggested that the *Lamr1* gene family in mammals, with the exception of the functional locus, is comprised entirely of retrotransposons or processed pseudogenes. Most processed retroposons are not expressed and have no functional activity, but several active retroposons or pseudogenes have been identified[29–32]. We show that the active retroposon may cause the pathological condition of ARVD. In humans, a highly conserved mutated form of *Lamr1* has been isolated from a fetal brain cDNA library[33], suggesting that mutant LAMR1 proteins are also transcribed in humans. Several reported human ARVD loci are located

close to the retroposons of *Lamr1* or histone-modulating protein genes (Table 1), suggesting that either LAMR1 or HP1 may cause hereditary RVD in humans.

METHODS

PWK mouse strain. The PWK strain belongs to the *Mus musculus musculus* subspecies, which separated from *Mus musculus domesticus* some 1 million years ago. It is maintained as one of the wild-type–derived inbred strains.

Lamr1-tp1 expressional analysis. We carried out PCR assays to confirm the presence of each identified mutation. Mismatch assays for the 287T→C and 291G→T mutations in the nucleic acid sequence of *Lamr1* introduced changes at the penultimate 3′ position for the forward primer and 868C→T for the reverse primer, respectively (primer sequences available on request). Each PCR product was digested with *Nhe*I (specific for *Lamr1-tp1* amplicon) to produce fragments of 334 bp and 279 bp; the *Lamr1* amplicon was uncut.

Injection of recombinant DNA *in vivo*. Female C57Bl/6 mice (8 weeks old, 22–25 g) were anesthetized with a mixture of ketamine (100 mg per kg body weight intraperitoneally) and xylazine (5 mg kg body weight intraperitoneally), intubated and ventilated. We carried out a left lateral thoracotomy to expose the beating heart and injected 10 μg of plasmid DNA in 100 μl of phosphate-buffered saline containing 5% sucrose into the right ventricular wall with a 30-gauge needle. The mice were killed 3 weeks after injection and histological staining was done.

Transgenic mice models. We constructed three kinds of targeting vectors under the following promoters (*Lamr1-tp1*, KSCX and α-MHC; *Lamr1*, α-MHC). We introduced these targeting vectors into blastocysts (derived from the C57Bl/6 Jcl mouse strain) by a standard pronuclear microinjection technique[34].

Preparation of adenovirus. Replication-defective recombinant adenoviral vectors expressing Lamr1-tp1-IRES-GFP and Lamr1-IRES-GFP were prepared with the adenovirus expression vector kit following the manufacturer's protocol (Takara). Briefly, *Lamr1-tp1* and *Lamr1* cDNA connected to an IRES-GFP sequence (Clontech) were placed after a CA promoter that was composed of a cytomegalovirus enhancer; a chicken β-actin promoter and rabbit β-globin poly(A) were inserted into a cassette cosmid vector that contained an entire adenovirus type 5 genome except for the E1a, E1b and E3 regions. A recombinant adenovirus was constructed by *in vitro* homologous recombination in HEK293 cells with the use of this cosmid vector and the adenovirus DNA terminal-protein complex. The desired recombinant adenovirus was purified by ultracentrifugation through a CsCl₂ gradient followed by extensive dialysis. The titer of the virus stock was assessed by a plaque formation assay that used the HEK293 cells. Cardiomyocytes were infected with the recombinant adenovirus vectors at a multiplicity of infection of 5–100 plaque-forming units per cell. We assessed the expression of GFP and β-actin by immunoblotting with 20 μg of myocardial protein lysate.

Primary culture of neonatal rat ventricular myocytes and MTS assay. Ventricular myocytes obtained from 1- or 2-d-old Wister rats were prepared and cultured overnight in Dulbecco's modified Eagle medium containing 10% fetal bovine serum as described[35]. Cytotoxicity was assessed with a CellTiter 96 Aqueous One Solution Cell Proliferation Assay System (Promega). Rat cardiomyocytes were cultured in 96-well culture plates at a density of 3×10^4 cells cm⁻². MTS reagent was added to each well 48 h after the addition of adenovirus to the myocytes. After a 1-h incubation period, optical absorbance at 490 nm was measured with a microplate reader. Cell viability was expressed as mean percentages for the absorbance at multiplicity of infection of 5 with the standard deviations of absorbance.

Antibodies. We used antibodies to MCP-1 (Santa Cruz Biotechnology), GFP, Myc-conjugate beads (Clontech), V₅ (Invitrogen) and HP1-α (Upstate Biotechnology). The polyclonal antibody FD4818 was derived from rabbits against the amino acid sequence RALNVLQMKEEDVFK, which corresponds to amino acids 3–15 of LAMR1.

Identification of LAMR1-TP1 binding protein (RVAP27). We metabolically labeled 2.0×10^5 COS7 cells expressing either PCDNA3.1-Myc-tagged-Lamr1 or PCDNA3.1-Myc-tagged-Lamr1-tp1 (Invitrogen) with ^{35}S, lysed them with 1 ml of lysis buffer (20 mM Tris pH 8.0, 5% acetonitrile, 5 M MEDTA, 1% Nonidet P-40) and immunoprecipitated them with a Myc antibody. Bound materials were separated by SDS-PAGE and the radioactivity was detected by a BAS imaging analyzer (Fuji). The eluted fraction from Myc-antibody beads was also injected onto a Phenyl-RPLC column (4.6×250mm, Nakarai) equilibrated with 0.1% trifluoroacetic acid and 5% acetonitrile. Fractions were eluted with a linear gradient of 27–37% acetonitrile at a flow rate of 1 ml. Each fraction was lyophilized and separated by SDS-PAGE. Radioactivity was detected by BAS imaging system.

Large-scale purification and sequence analysis of LAMR1-TP1–binding protein. COS7 cells (1.0×10^8) expressing Myc-tagged LAMR1-TP1 were lysed with 200 ml of lysis buffer and applied to 500 μl of Myc-antibody beads (Clontech). Bound materials were eluted with 0.1% trifluoroacetic acid and 5% acetonitrile. The eluted fraction was diluted 50 times with a lysis buffer and was applied to Uno-Q anion exchange column (Bio-Rad). The column was equilibrated with 20 mM Tris and 5% acetonitrile at pH 8.0 and bound materials were eluted with a linear gradient of NaCl (0–0.5 M) at a flow rate of 1 ml min^{-1}. Five fractions of about 0.3 M NaCl elution were pooled and injected onto a Phenyl-RPLC column (4.6×250 mm, Nakarai) equilibrated with 0.1% trifluoroacetic acid and 5% acetonitrile. Fractions were eluted with a linear gradient of 27–37% acetonitrile at a flow rate of 1 ml. After separating by SDS-PAGE, RVAP27 was eluted at the same fraction in which the radioactive LAMR1-TP1 was detected. Purified RVAP (10 pmol) was subjected to SDS-PAGE on 12% gel. After staining the gel with SyproRuby, the 27-kDa band was cut and treated with trypsin. The tryptic digest was fractionated by nanoscale HPLC on a C18 column (0.1×50 mm). Two fractions were analyzed by direct N-terminal sequence by Edman degradation with the HP G1005 Protein Sequencing System. One fraction was analyzed with a tandem mass spectrometer (Q-Tof2) equipped with a nanoelectrospray ionization source. Positive ion tandem mass spectra were measured.

RNA preparation and hybridization to oligonucleotide arrays. Total RNA was isolated from viable mice or cultured neonatal cardiomyocytes derived from C57Bl/6 mice. Affymetrix Gene Chip technology was used as described[36]. Briefly, cDNA was synthesized from total RNA and annealed to a T7-oligo-dT primer. Reverse transcription was done with Superscript II reverse transcriptase. Second-strand cDNA synthesis was done with DNA polymerase I with the appropriate reagents. Synthesis of biotin-labeled cRNA was done by *in vitro* transcription with the MEGAscript T7 IVT Kit (Ambion, Inc). The cRNA was fragmented and hybridized to GeneChip Murine U74vA2 Array Set (Affymetrix). Hybridization, probe washing, staining and probe array scan were done according to the protocols provided by Affymetrix. Detailed information about the array protocol and data is available in the GEO database (see URL and accession number below).

Real-time PCR. Real-time PCR was done with TaqMan technology and the ABI Prism 7700 Detection System (Applied Biosystems). Reactions (25 μl) were set up using the 2× Universal PCR Master Mix (Applied Biosystems), template cDNA and adequate concentrations of primers and probes. All of the samples were processed in duplicate. To standardize the quantity of the two selected genes, GAPDH was used as the endogenous control reference because our microarray analysis showed that the level of GAPDH was stable and no significant difference was noted among all the three groups.

Data analysis. GeneSpring 5.0 (Silicon Genetics) software was used for analyses. A global normalization was used for all data in the 18 arrays with a combination of three steps: transforming negative values to 0.01, normalizing to the 50th percentile per chip and normalizing to median per gene. We filtered data using a combination of signal confidence ('present' flag), relative change (1.5–2.0 times), minimum acceptable signal intensity (average difference ≥ 50 in at least one of three groups) and a statistical cut-off ($P < 0.05$, Student's *t*-test). Data are presented as mean or mean $\pm$ s.e.m.; the one-way ANOVA with Tukey-Kramer exact probability test was used to test the differences among all

the groups and the least-squares method was used to determine linear correlation between selected variables. $P < 0.05$ was considered statistically significant.

Animal experiments. All animal experiments were approved by the Institutional Animal Care and Use Committee at Osaka University Graduate School of Medicine.

URL. The GEO database is available at http://www.ncbi.nlm.nih.gov/geo/.

GEO accession number. GSE927.

Note: Supplementary information is available on the Nature Genetics website.

1. Thiene, G. *et al.* Arrythmogenic right ventricular cardiomyopathy. *Trends Cardiovasc. Med.* 7, 84–90 (1997).
2. Severini, G.M. *et al.* A new locus for arrhythmogenic right ventricular dysplasia on the long arm of chromosome 14. *Genomics* 31, 193–200 (1996).
3. Rampazzo, A. *et al.* ARVD4, a new locus for arrhythmogenic right ventricular cardiomyopathy, maps to chromosome 2 long arm. *Genomics* 45, 259-263 (1997).
4. Ahmad, F. *et al.* Localization of a gene responsible for arrhythmogenic right ventricular dysplasia to chromosome 3p23. *Circulation* 98, 2791 2795 (1998).
5. Li, D. *et al.* The locus of a novel gene responsible for arrhythmogenic right- ventricular dysplasia characterized by early onset and high penetrance maps to chromosome 10p12-p14. *Am. J. Hum. Genet.* 66, 148–156 (2000).
6. Tiso, N. *et al.* Identification of mutations in the cardiac ryanodine receptor gene in families affected with arrhythmogenic right ventricular cardiomyopathy type 2 (ARVD2). *Hum. Mol. Genet.* 10, 189-194 (2001).
7. Bright, J.M. & McEntee, M. Isolated right ventricular cardiomyopathy in a dog. *J. Am. Vet. Med. Assoc.* 207, 64–66 (1995).
8. Simpson, K.W., Bonagura, J.D. & Eaton, K.A. Right ventricular cardiomyopathy in a dog. *J. Vet. Intern. Med.* 8, 306–309 (1994).
9. Fox, P.R., Maron, B.J., Basso, C., Liu, S.K. & Thiene, G. Spontaneously occurring arrhythmogenic right ventricular cardiomyopathy in the domestic cat: A new animal model similar to the human disease. *Circulation* 102, 1863–1870 (2000).
10. Ishikawa, S., Zu Rhein, G.M. & Gilbert, E.F. Uhl's anomaly in the mink. Partial absence of the right atrial and ventricular myocardium. *Arch. Pathol. Lab. Med.* 101, 388–390 (1977).
11. Sato, M. *et al.* Analysis of nuclear localization of laminin binding protein precursor p40 (LBP/p40). *Biochem. Biophys. Res. Commun.* 229, 896–901 (1996).
12. Kaneda, Y. *et al.* The induction of apoptosis in HeLa cells by the loss of LBP-p40. *Cell Death Differ.* 5, 20–28 (1998).
13. Kondo, K., Nozawa, K., Tomita, T. & Ezaki, K. Inbred strains resulting from Japanese mice. *Bull. Exp. Anim.* 6, 107–112 (1967).
14. Nakamura, M. & Yamada, K. Studies on a diabetic (KK) strain of the mouse. *Diabetologia* 3, 212–221 (1967).
15. McKenna, W.J. *et al.* Diagnosis of arrhythmogenic right ventricular dysplasia/cardiomyopathy. Task Force of the Working Group Myocardial and Pericardial Disease of the European Society of Cardiology and of the Scientific Council on Cardiomyopathies of the International Society and Federation of Cardiology. *Br. Heart J.* 71, 215–218 (1994).
16. Lin, H., Parmacek, M.S., Morle, G., Bolling, S. & Leiden, J.M. Expression of recombinant genes in myocardium in vivo after direct injection of DNA. *Circulation* 82, 2217–2221 (1990).
17. Nakayama, J., Rice, J.C., Strahl, B.D., Allis, C.D. & Grewal, S.I. Role of histone H3 lysine 9 methylation in epigenetic control of heterochromatin assembly. *Science* 292, 110–113 (2001).
18. Festenstein, R. *et al.* Modulation of heterochromatin protein 1 dynamics in primary Mammalian cells. *Science* 299, 719–721 (2003).
19. Cranefield, P. *The Conduction of the Cardiac Impulse* (Futura, Mount Kisco, New York, 1975).
20. Peters, S. & Trummel, M. Diagnosis of arrhythmogenic right ventricular dysplasia-cardiomyopathy: value of standard ECG revisited. *Ann. Noninvasive Electrocardiol.* 8, 238–245 (2003).

ARTICLES

21. Nasir, K. *et al.* Filtered QRS duration on signal-averaged electrocardiography predicts inducibility of ventricular tachycardia in arrhythmogenic right ventricle dysplasia. *Pacing Clin. Electrophysiol.* **26**, 1955–1960 (2003).
22. Burke, A.P., Farb, A., Tashko, G. & Virmani, R. Arrhythmogenic right ventricular cardiomyopathy and fatty replacement of the right ventricular myocardium: are they different diseases? *Circulation* **97**, 1571–1580 (1998).
23. Protonotarios, N. *et al.* Genotype-phenotype assessment in autosomal recessive arrhythmogenic right ventricular cardiomyopathy (Naxos disease) caused by a deletion in plakoglobin. *J. Am. Coll. Cardiol.* **38**, 1477–1484 (2001).
24. Steenman, M. *et al.* Transcriptomal analysis of failing and nonfailing human hearts. *Physiol. Genomics* **12**, 97–112 (2003).
25. Pashmforoush, M. *et al.* Adult mice deficient in actinin-associated LIM-domain protein reveal a developmental pathway for right ventricular cardiomyopathy. *Nat. Med.* **7**, 591–597 (2001).
26. Cheutin, T. *et al.* Maintenance of stable heterochromatin domains by dynamic HP1 binding. *Science* **299**, 721–725 (2003).
27. Zhang, C.L. *et al.* Class II histone deacetylases act as signal-responsive repressors of cardiac hypertrophy. *Cell* **110**, 479–488 (2002).
28. Zhang, C.L., McKinsey, T.A. & Olson, E.N. Association of class II histone deacetylases with heterochromatin protein 1: potential role for histone methylation in control of muscle differentiation. *Mol. Cell. Biol.* **22**, 7302–7312 (2002).
29. McCarrey, J.R. & Thomas, K. Human testis-specific PGK gene lacks introns and possesses characteristics of a processed gene. *Nature* **326**, 501–505 (1987).
30. Gebara, M.M. & McCarrey, J.R. Protein-DNA interactions associated with the onset of testis-specific expression of the mammalian Pgk-2 gene. *Mol. Cell. Biol.* **12**, 1422-1431 (1992).
31. Dahl, H.H., Brown, R.M., Hutchison, W.M., Maragos, C. & Brown, G.K. A testis-specific form of the human pyruvate dehydrogenase E1 α subunit is coded for by an intronless gene on chromosome 4. *Genomics* **8**, 225–232 (1990).
32. Hirotsune, S. *et al.* An expressed pseudogene regulates the messenger-RNA stability of its homologous coding gene. *Nature* **423**, 91–96 (2003).
33. Richardson, M.P., Braybrook, C., Tham, M., Moore, G.E. & Stanier, P. Molecular cloning and characterization of a highly conserved human 67- kDa laminin receptor pseudogene mapping to Xq21.3. *Gene* **206**, 145-150 (1998).
34. Gordon, J.W., Scangos, G.A., Plotkin, D.J., Barbosa, J.A. & Ruddle, F.H. Genetic transformation of mouse embryos by microinjection of purified DNA. *Proc. Natl. Acad. Sci. USA* **77**, 7380–7384 (1980).
35. Simpson, P., McGrath, A. & Savion, S. Myocyte hypertrophy in neonatal rat heart cultures and its regulation by serum and by catecholamines. *Circ. Res.* **51**, 787–801 (1982).
36. Lockhart, D.J. *et al.* Expression monitoring by hybridization to high-density oligonucleotide arrays. *Nat. Biotechnol.* **14**, 1675–1680 (1996).

BBRC

Roles of charged amino acid residues in the cytoplasmic domain of proHB-EGF

Daisuke Nanba,[a] Fujio Toki,[a,b] and Shigeki Higashiyama[a,c,*]

[a] Division of Biochemistry and Molecular Genetics, Department of Molecular and Cellular Biology, Ehime University School of Medicine,
Shitsukawa, Shigenobu-cho, Onsen-gun, Ehime 791-0295, Japan
[b] Department of Molecular Pathology, School of Allied Health Sciences, Osaka University, Suita, Osaka 565-0871, Japan
[c] PRESTO, JST, Japan

Abstract

Heparin-binding EGF-like growth factor (HB-EGF) is initially synthesized as a type I transmembrane precursor (proHB-EGF). Proteolytic cleavage of proHB-EGF yields amino- and carboxy-terminal fragments (HB-EGF and HB-EGF-C, respectively). We have previously shown that HB-EGF-C is translocated from the plasma membrane into the nucleus, where it interacts with the transcription repressor, PLZF. Here we characterize the amino acid residues of the cytoplasmic domain of proHB-EGF on cell surface distribution and the interaction of HB-EGF-C with PLZF. The cytoplasmic domain contains three characteristic clusters with charged amino acids. Generation of various mutants of proHB-EGF showed that the arrangement of the charged amino acids in the cytoplasmic domain regulates the distribution of proHB-EGF at the plasma membrane but does not regulate proHB-EGF processing and internalization of HB-EGF-C. Further, the charged amino acids are also required for HB-EGF-C–PLZF interaction. These results indicate that the cytoplasmic domain of proHB-EGF is a multifunctional domain.
© 2004 Elsevier Inc. All rights reserved.

Keywords: HB-EGF; PLZF; EGF family; Intracellular signaling; Membrane-anchored growth factor

Heparin-binding EGF-like growth factor (HB-EGF) is a member of the EGF family that was first identified as a secreted product of macrophages and macrophage-like U-937 cells [1]. It is a 20–22 kDa glycoprotein found in multiple forms of 76–86 amino acids [2]. HB-EGF binds directly to the EGF receptor (EGFR)/ErbB1 [1] and ErbB4 [3], activates ErbB2 indirectly by receptor heterodimerization [4], and induces ErbBs signaling in cells. N-Arginine dibasic convertase (NRDc) has been also identified as a specific cell surface receptor for HB-EGF that enhances cell migration in response to HB-EGF via EGFR [5].

A structural feature common to all members of the EGF family is their synthesis via a precursor molecule that is tethered to the plasma membrane via a trans-membrane domain [6]. Before HB-EGF is secreted by

cells, it is processed from a 208 amino acid precursor composed of various domains (e.g., signal peptide, pro-peptide, heparin-binding, EGF-like, transmembrane, and cytoplasmic) [1,2]. The membrane-anchored precursor of HB-EGF (proHB-EGF) exerts its bioactivity in two distinct ways: it serves a receptor for diphtheria toxin [7], a specific function not shared by other EGF family members [8,9], and it stimulates growth of adjacent cells [10].

Newly synthesized proHB-EGF molecules first undergo amino-terminal processing at Arg^{62}-Asp^{63} by the endoprotease, furin [11]. Next, cleavage at a Pro^{149}-Val^{150} by "a disintegrin and metalloprotease" (ADAM) molecules and matrix metalloproteases [12,13] takes place to release a soluble form of HB-EGF. This cleavage can be stimulated by various regents, including the phorbol ester 12-O-tetradecanoylphorbol-13-acetate (TPA) [14]. The processing of the extracellular domain, which is termed "ectodomain shedding," also creates a

* Corresponding author. Fax: +81-89-960-5256.
E-mail address: shigeki@m.ehime-u.ac.jp (S. Higashiyama).

remnant carboxy-terminal cell-associated fragment (HB-EGF-C) consisting of juxtamembrane, transmembrane, and cytoplasmic domains.

We recently reported that HB-EGF-C interacts with a nuclear transcriptional repressor, promyelocytic leukemia zinc finger (PLZF), and evokes a novel intracellular signaling pathway that is independent of EGFR activation [15]. HB-EGF-C–PLZF interaction is mediated by the cytoplasmic domain of proHB-EGF. In addition, neuregulin-1, a member of the family of EGF molecules, is cleaved at the transmembrane domain. The intracellular domain (Nrg-1-ICD) released from this process regulates gene transcription [16]. These findings indicate that the cytoplasmic domain of the membrane-anchored precursor of the EGF family molecules is a functional domain.

Here we characterize amino acid residues of the cytoplasmic domain for the distribution of proHB-EGF on cell surface and the interaction of HB-EGF-C with PLZF. The specific sequences of amino acid residues of the cytoplasmic domain were required for proHB-EGF distribution at plasma membrane and the interaction of HB-EGF-C with PLZF after proHB-EGF processing. These results indicate that the cytoplasmic tail of proHB-EGF is a multifunctional domain.

Materials and methods

Plasmid construction. Plasmids for recombinant expression of YFP-tagged proHB-EGF, CFP-tagged PLZF, and FLAG-tagged PLZF were described previously [15]. DNA fragments encoding the deleted or mutant cytoplasmic region of proHB-EGF (with or without the stop codon deleted) were generated by PCR and substituted for the corresponding region of pEYFP-N1-proHB-EGF [15]. Plasmids for recombinant expression of GST-fused HB-TMC and HB-TMCM were generated by subcloning the *Bam*HI–*Eco*RI fragment containing the transmembrane and cytoplasmic domain sequence made by PCR at the *Bam*HI/*Eco*RI sites of pGEX6P-1 (Amersham Biosciences). All cDNA constructs were purified by QIAGEN Plasmid Maxi kit and verified by DNA sequence.

Cell lines and transfection. Preparation and maintenance of HT1080/proHB-EGF cells was described previously [15]. For the establishment of HT1080/proHBcytoM cells, the plasmids encoding proHBcytoM mutants were introduced into HT1080 cells using Lipofectamine 2000 (Invitrogen), and stably transfected clones were isolated. HT1080 cells were grown in Eagle-MEM supplemented with non-essential amino acids (Invitrogen), 10% fetal bovine serum (FBS), and antibiotics. Stable transfectants were maintained in the same medium with 1 mg/ml G418. All cells were cultured in a humidified 37 °C/5% CO_2 incubator.

For transient transfections, 4.0×10^5 cells were seeded in 35-mm cell-culture dishes (CORNING), grown for 12 h in medium, and then transfected with expression vectors using Lipofectamine 2000 (Invitrogen).

Immunoblotting. Immunoblotting was performed as described previously [14]. Primary antibodies were used as follows: rabbit polyclonal antibody to GFP (MBL International Corporation) and mouse monoclonal antibody to FLAG (Sigma–Aldrich). Secondary antibodies were HRP-conjugated goat anti-mouse and rabbit IgG.

Imaging of YFP- and CFP-tagged protein and immunofluorescence microscopy. The assessment of subcellular localization of YFP- or CFP-fusion proteins and immunofluorescence microscopy were per-

formed as described previously [15]. The following primary antibodies were used: a goat polyclonal antibody to clathrin (Sigma–Aldrich) and a mouse monoclonal antibody to caveolin-1 (BD Transduction Laboratories). The following secondary antibodies were used: rhodamine-conjugated donkey anti-goat IgG and rhodamine-conjugated goat anti-mouse IgG (CHEMICON). Some cells were also stained with Hoechst 33258 (Molecular probes)

GST pull-down assay. GST, GST-HB-TMC, and GST-HB-TMCM were expressed in and purified from the *E. coli* BL21 strain according to standard protocol. GST pull-down assay was performed as previously described [15].
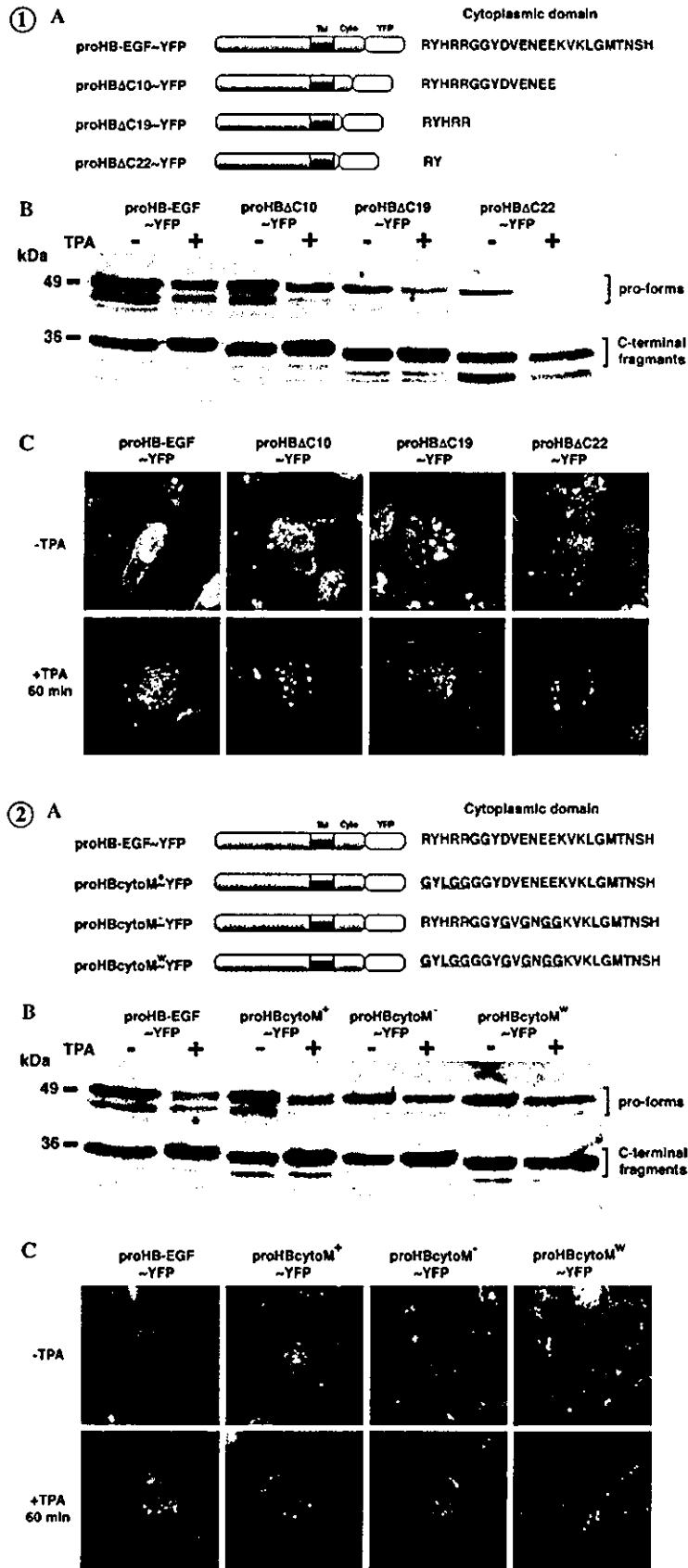
Results

Cytoplasmic structure of proHB-EGF

The cytoplasmic domain of proHB-EGF consists of 24 amino acids with three characteristic clusters of charged amino acid residues; the first is a positively charged cluster (RYHRR), the second is a negatively charged cluster (DVENEE), and the third is a positively charged cluster (KVK) (Figs. 1A and 2A).

Processing and distribution of proHB-EGF truncated mutants

Recombinant protein in which YFP was fused to the carboxy-terminus of proHB-EGF (proHB-EGF~YFP) was synthesized as an expected size, distributed at the plasma membrane, and proteolytically cleaved after TPA treatment (Figs. 1B and C). To investigate the role of the cytoplasmic domain on proHB-EGF processing and subcellular localization, we first constructed plasmids encoding three types of YFP-tagged cytoplasmic deletion mutants of proHB-EGF (proHBΔC10~YFP, proHBΔC19~YFP, and proHBΔC22~YFP; Fig. 1A). These expression plasmids were transiently transfected into human fibrosarcoma HT1080 cells, and the fusion proteins were detected by immunoblotting using anti-GFP antibody after the treatment with or without 100 nM TPA for 60 min. All YFP fusion proteins were detected as heterogeneous bands at ~49 and ~36 kDa, respectively (Fig. 1B). Pro-forms of these recombinant proteins were detected as ~49 kDa bands in each lane. After TPA stimulation, carboxy-terminal fragments of these pro-forms were detected as ~36 kDa bands in each lane. TPA treatment decreased the intensity of the ~49 kDa bands in the three types of the truncated mutants as well as in proHB-EGF~YFP. This suggests that these truncated mutants are processed normally in response to TPA stimulation.

The distribution of YFP-fusion proHB-EGF variants was assessed using a fluorescent microscope. In the absence of TPA, all fusions were mainly localized at the plasma membrane. While proHB-EGF~YFP and proHBΔC10~YFP were distributed homogeneously throughout the plasma membrane, cells expressing

① A

Cytoplasmic domain

proHB-EGF~YFP		RYHRRGGYDVENEEKVKLGMTNSH
proHBΔC10~YFP		RYHRRGGYDVENEE
proHBΔC19~YFP		RYHRR
proHBΔC22~YFP		RY

B

C

② A

Cytoplasmic domain

proHB-EGF~YFP		RYHRRGGYDVENEEKVKLGMTNSH
proHBcytoM⁺~YFP		GYLGGGGYDVENEEKVKLGMTNSH
proHBcytoM⁻~YFP		RYHRRGGYGVGNGGKVKLGMTNSH
proHBcytoMᵂ~YFP		GYLGGGGYGVGNGGKVKLGMTNSH

B

C

proHBΔC19~YFP and proHBΔC22~YFP had patches of the YFP-fusion proteins at the plasma membrane (Fig. 1C). After TPA treatment, the carboxy-terminal fragments of all fusion proteins were localized around the nucleus (Fig. 1C).

Processing and distribution of proHB-EGF cytoplasmic uncharged mutants

The proHB-EGF cytoplasmic domain contains three clusters of charged amino acids (Fig. 2A). To investigate the roles of these charged clusters, we generated three types of proHB-EGF~YFP uncharged mutants by replacing clusters of charged amino acids with those of uncharged amino acids (proHBcytoM$^+$~YFP and proHBcytoM$^-$~YFP, and proHBcytoM^w~YFP; Fig. 2A). The plasmids encoding proHB-EGF~YFP and three types of uncharged mutants were transiently transfected into HT1080 cells, and the recombinant proteins were detected by immunoblotting with an anti-GFP antibody after incubation in medium with or without TPA. All three mutant proteins and proHB-EGF~YFP underwent normal processing in response to TPA stimulation (Fig. 2B).

The subcellular localization of recombinant YFP fusion was assessed under a fluorescent microscope. When the transfected cells were incubated with normal medium, proHB-EGF~YFP was distributed homogeneously throughout the plasma membrane. In contrast, cells transfected with three types of mutants showed patch-like distribution of YFP-fused mutant proteins (Fig. 2C). Following treatment with TPA, the cells expressing proHB-EGF~YFP and its mutants showed carboxy-terminal fragments distribution around the nucleus (Fig. 2C).

HB-EGF-C internalization is mediated by clathrin-dependent endocytosis

The images of truncated mutants of proHB-EGF~YFP after TPA treatment indicate that the cyto-plasmic domain is not necessary for the internalization of HB-EGF-C. HB-EGF-C retains the transmembrane domain [15] and, therefore, can be carried into the cytoplasm by a vesicle trafficking mechanism, such as clathrin- and caveolin-mediated endocytosis. To test this possibility, we performed immunostaining with antibodies against clathrin and caveolin-1 in HT1080 cells transiently expressing proHB-EGF~YFP. ProHB-EGF~YFP was localized to the plasma membrane. After TPA treatment for 30 min, the carboxy-terminal fragments of proHB-EGF~YFP (HB-EGF-C~YFP) were localized around the nucleus. In this condition, HB-EGF-C~YFP co-localized with clathrin but not with caveolin-1 (Figs. 3A and B). These results indicate that HB-EGF-C containing the transmembrane domain is internalized into the cytoplasm by a process that is at least partially dependent on clathrin-mediated endocytosis.

Charged amino acid residues in the cytoplasmic domain of proHB-EGF are essential for PLZF export induced by proHB-EGF processing

We have previously reported that the cytoplasmic domain of proHB-EGF is required for PLZF export from the nucleus [15]. To investigate the effect of charged amino acid clusters in the cytoplasmic domain, we established HT1080 cells stably expressing proHB-EGF, proHBcytoM$^+$, proHBcytoM$^-$, and proHBcytoM^w (Fig. 4A). The plasmid for recombinant expression of CFP~PLZF was transiently transfected into HT1080 cells and its variants, and images of the CFP-fusion protein were collected with or without the treatment with 100 nM TPA for 60 min. In all cell types, CFP~PLZF was predominantly localized at the nucleus before TPA stimulation (Figs. 4B and C). TPA treatment resulted in distribution of CFP~PLZF throughout the entire cytoplasm of HT1080/proHB-EGF cells (Figs. 4B and C), as previously reported [15]. In HT1080/proHBcytoM$^+$ and HT1080/proHBcytoM$^-$ cells, however, the nuclear export of CFP~PLZF after TPA treatment was partially inhibited (Figs. 4B and C). Furthermore, in HT1080/

Fig. 1. Processing and distribution of proHB-EGF truncated mutants. (A) Schematic structure of proHB-EGF~YFP truncated mutants. (B) Expression of YFP-fusion proteins was detected by immunoblotting with anti-GFP antibody. The ~49 kDa band of pro-form of each YFP-fusion protein was decreased by the TPA stimulation. In contrast, the ~36 kDa band of the carboxy-terminal fragment from each YFP-fusion pro-form (C-terminal fragment) was increased after the treatment. (C) Distribution of YFP-fusion proteins (green) and nucleus (blue). ProHB-EGF~YFP and proHBΔC10~YFP were distributed homogeneously throughout the plasma membrane, while proHBΔC19~YFP and proHBΔC22~YFP showed patch-like distribution in the plasma membrane. The carboxy-terminal fragments of proHB-EGF~YFP and its variants generated by the TPA treatment were localized around the nucleus. Bar = 10 μm.

Fig. 2. Processing and distribution of proHB-EGF cytoplasmic uncharged mutants. (A) Schematic structure of proHB-EGF~YFP cytoplasmic uncharged mutants. (B) Expression of YFP-fusion proteins was detected by immunoblotting with anti-GFP antibody. The band of pro-form of each YFP-fusion protein decreased in response to TPA stimulation. In contrast, the band of the carboxy-terminal fragment of each YFP-fusion pro-form (C-terminal fragment) increased in response to treatment. (C) Distribution of YFP-fusion proteins (green) and nucleus (blue). ProHB-EGF~YFP was distributed homogeneously throughout the plasma membrane, while the three types of cytoplasmic uncharged mutants were distributed in a patch-like fashion in the plasma membrane. The carboxy-terminal fragments of proHB-EGF~YFP and its variants generated by the TPA treatment were localized around the nucleus. Bar = 10 μm.
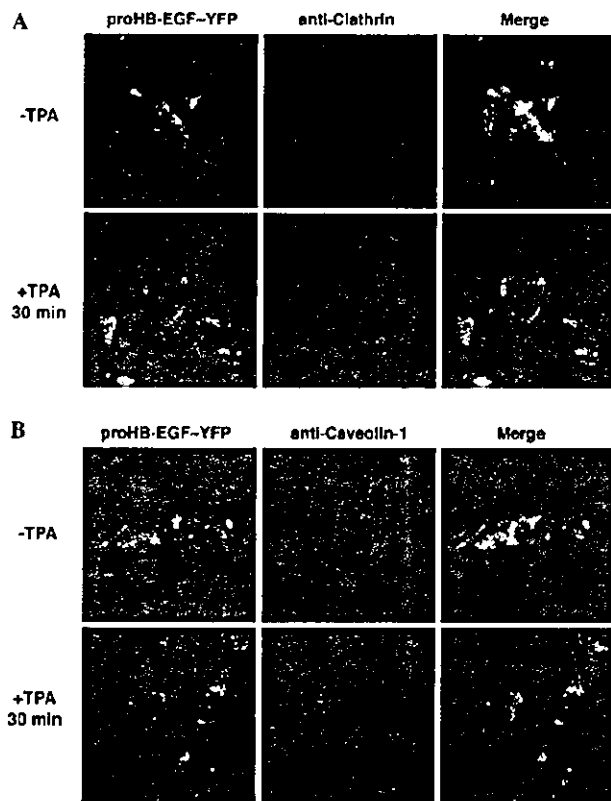
Fig. 3. Colocalization of the carboxy-terminal fragment of proHB-EGF∼YFP (HB-EGF-C∼YFP) with clathrin following TPA treatment. (A,B) HT1080 cells transiently expressing proHB-EGF∼YFP were immunostained with anti-clathrin and caveolin-1 antibodies, respectively, before and after TPA stimulation. (A) After the treatment, HB-EGF-C∼YFP colocalized with clathrin around the nucleus. (B) Colocalization of HB-EGF-C∼YFP with caveolin-1 was not observed following TPA treatment. Bars = 10 μm.

proHBcytoM^w cells, the degree of PLZF export was greatly reduced (Figs. 4B and C).

Sequence specific required for interaction of HB-EGF-C with PLZF

Interaction between PLZF and HB-EGF-C is required for PLZF export [15]. We investigated the binding of PLZF with HB-EGF-C containing wild-type- or an uncharged mutant cytoplasmic domain using a GST pull-down assay. Glutathione–Sepharose beads conjugated either with GST alone, with recombinant fragments containing transmembrane and cytoplasmic domain of proHB-EGF fused to GST (GST-HB-TMC), or with recombinant fragments containing transmembrane and uncharged mutant cytoplasmic domain fused to GST (GST-HB-TMCM) (Figs. 5A and B) were generated. Next, cell lysate containing FLAG-tagged PLZF was incubated with these beads. PLZF associated with GST-HB-TMC, but not with GST alone or with GST-HB-TMCM (Fig. 5C).
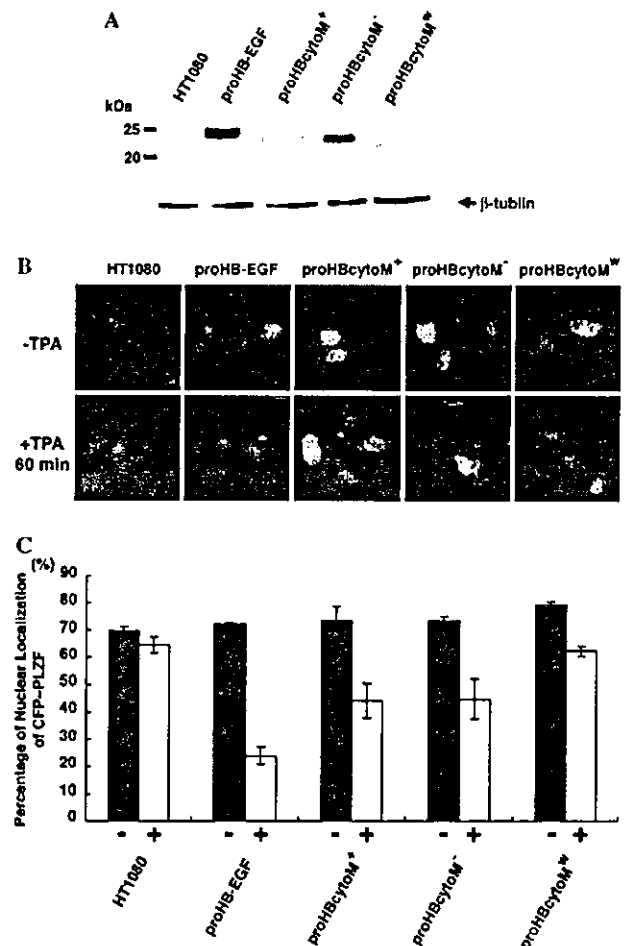

Fig. 4. ProHB-EGF processing-dependent nuclear export of PLZF requires charged clusters in the cytoplasmic domain of proHB-EGF. (A) HT1080 cells stably expressing proHB-EGF, proHBcytoM$^+$, proHBcytoM$^-$, and proHBcytoM^w were established. Expression of proHB-EGF and its variants confirmed by immunoblotting with anti-HB-EGF antibody (upper panel). The expression of β-tubulin was used as control (lower panel). (B,C) Subcellular localization of CFP∼PLZF fusion protein in HT1080 cells and its variants. CFP∼PLZF expression vector was transiently transfected into HT1080 cells and its transfectants. CFP∼PLZF was predominantly localized to the nucleus in these cell types. In HT1080/proHB-EGF but not in parental HT1080 cells, CFP∼PLZF was distributed in the entire cytoplasm following treatment with 100 nM TPA. In HT1080/proHBcytoM$^+$ and HT1080/proHBcytoM$^-$ cells, the nuclear export of CFP∼PLZF was partially inhibited. The degree of CFP∼PLZF export was greatly decreased in HT1080/proHBcytoM^w cells.

Discussion

We have previously shown that HB-EGF-C is translocated from the plasma membrane to the nucleus after proHB-EGF processing and that HB-EGF-C interacts with PLZF [15]. The present study demonstrated that the cytoplasmic domain of proHB-EGF plays a key role in proHB-EGF distribution and HB-EGF-C–PLZF interaction.
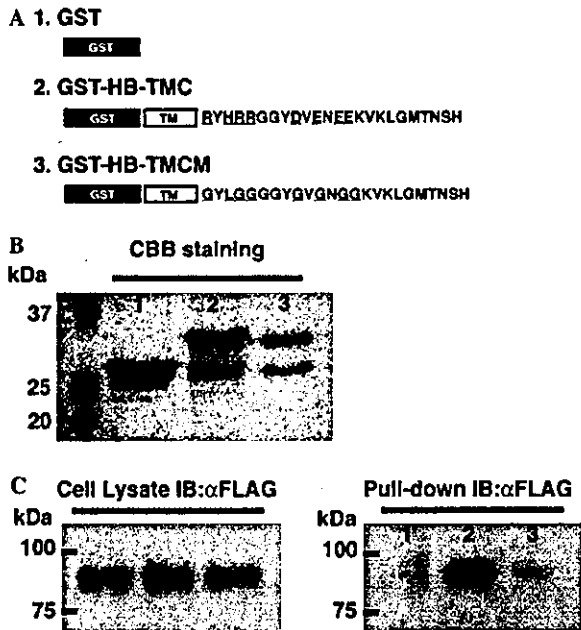
A 1. GST

GST

2. GST-HB-TMC

GST TM RYHBBGGYDVENEEKVKLGMTNSH

3. GST-HB-TMCM

GST TM QYLGGGGYGVGNGQKVKLGMTNSH

B   CBB staining
kDa

37

25
20

C   Cell Lysate IB:αFLAG   Pull-down IB:αFLAG
kDa   kDa
100   100

75   75

Fig. 5. Sequence specific interaction of the cytoplasmic domain of proHB-EGF with PLZF. (A) Schematic structures of GST alone, GST-HB-TMC, and GST-HB-TMCM. (B) GST (1), GST-HB-TMC (2), or GST-HB-TMCM (3) separated by SDS–PAGE were stained with CBB. (C) Cell lysates containing FLAG-tagged PLZF were incubated with GST (1), GST-HB-TMC (2), or GST-HB-TMCM (3) beads, and bound proteins were detected by immunoblotting with anti-FLAG antibody (right panel). Expression of FLAG-tagged PLZF was confirmed by immunoblotting using anti-FLAG antibody (left panel). FLAG-tagged PLZF was bound to GST-HB-TMC but not to GST alone or to GST-HB-TMCM.

In the present study we demonstrated that the cytoplasmic domain of proHB-EGF was not required for the proteolytic processing of proHB-EGF. This result is consistent with the report that the processing of precursors of HB-EGF and amphiregulin occurred in the absence of their cytoplasmic domain [17,18]. In this study, proHBΔC19~YFP and proHBΔC22~YFP showed patch-like distribution at the plasma membrane. In addition, cells transiently expressing three types of uncharged cytoplasmic mutants of proHB-EGF~YFP showed a similar type of distribution. These results indicate that the arrangement of the first positively and the second negatively charged clusters in the cytoplasmic domain is required for proper distribution of proHB-EGF at the plasma membrane.

The nuclear export of PLZF is dependent on proHB-EGF processing and requires the cytoplasmic domain of proHB-EGF [15]. Further, the present study demonstrated that the characteristic sequence of charged amino acid residues in the cytoplasmic domain of proHB-EGF was essential for interaction with PLZF and its subsequent nuclear export, but was not required for the translocation of HB-EGF-C. The presence of a transmembrane domain in HB-EGF-C [15] and

colocalization of HB-EGF-C with clathrin indicate that the internalization of HB-EGF-C is at least partially mediated by clathrin-dependent endocytosis. Precursors of other EGF family members also possess charged amino acid clusters in their cytoplasmic domains, suggesting that their carboxy-terminal fragments of their pro-forms can interact with PLZF or similar transcription repressors after their processing.

In conclusion, the cytoplasmic domain of proHB-EGF regulates proHB-EGF distribution at the plasma membrane, and the arrangement of charged amino acid clusters in the cytoplasmic domain is essential for HB-EGF-C-PLZF interaction. These results indicate that the cytoplasmic domain is a multifunctional domain. Focusing on the cytoplasmic domain of proHB-EGF and other EGF family precursors may be useful in the characterization of the functional diversity of EGF family molecules.

Acknowledgments

References

[1] S. Higashiyama, J.A. Abraham, J. Miller, J.C. Fiddes, M. Klagsbrun, A heparin-binding growth factor secreted by macrophage-like cells that is related to EGF, Science 251 (1991) 936–939.

[2] S. Higashiyama, K. Lau, G.E. Besner, J.A. Abraham, M. Klagsbrun, Structure of heparin-binding EGF-like growth factor: multiple forms, primary structure, and glycosylation of the mature protein, J. Biol. Chem. 267 (1992) 6205–6212.

[3] K. Elenius, S. Paul, G. Allison, J. Sun, M. Klagsbrun, Activation of HER4 by heparin-binding EGF-like growth factor stimulates chemotaxis but not proliferation, EMBO J. 16 (1997) 1268–1278.

[4] R. Iwamoto, S. Yamazaki, M. Asakura, S. Takashima, H. Hasuwa, K. Miyado, S. Adachi, M. Kitakaze, K. Hashimoto, G. Raab, D. Nanba, S. Higashiyama, M. Hori, M. Klagsbrun, E. Mekada, Heparin-binding EGF-like growth factor and ErbB signaling is essential for heart function, Proc. Natl. Acad. Sci. USA 100 (2003) 3221–3226.

[5] E. Nishi, A. Prat, V. Hospital, K. Elenius, M. Klagsbrun, N-Arginine dibasic convertase is a specific receptor for heparin-binding EGF-like growth factor that mediates cell migration, EMBO J. 20 (2001) 3342–3350.

[6] J. Massague, A. Pandiella, Membrane-anchored growth factors, Annu. Rev. Biochem. 62 (1993) 515–541.

[7] J.G. Naglich, J.E. Metherall, D.W. Russell, L. Eidels, Expression cloning of a diphtheria toxin receptor: identify with a heparin-binding EGF-like growth factor precursor, Cell 69 (1992) 1051–1061.

[8] R. Iwamoto, S. Higashiyama, T. Mitamura, N. Taniguchi, M. Klagsbrun, E. Mekada, Heparin-binding EGF-like growth factor, which acts as the diphtheria toxin receptor, forms a complex with membrane protein DRAP27/CD9, which up-regulates functional receptors and diphtheria toxin activity, EMBO J. 13 (1994) 2322–2330.

[9] T. Mitamura, S. Higashiyama, N. Taniguchi, M. Klagsbrum, E. Mekada, Diphtheria toxin binds to the EGF-like domain of human heparin-binding EGF-like growth factor/diphtheria toxin receptor and inhibits specifically its mitogenic activity, J. Biol. Chem. 270 (1995) 1015–1019.

[10] S. Higashiyama, R. Iwamoto, K. Goishi, G. Raab, N. Taniguchi, M. Klagsbrun, E. Mekada, The transmembrane protein CD9/DRAP27 potentiates the juxtacrine growth factor activity of the membrane-anchored heparin-binding EGF-like growth factor (proHB-EGF), J. Cell Biol. 128 (1995) 929–938.

[11] T. Nakagawa, S. Higashiyama, T. Mitamura, E. Mekada, N. Taniguchi, Amino-terminal processing of cell surface heparin-binding epidermal growth factor-like growth factor up-regulates its juxtacrine but not its paracrine growth activity, J. Biol. Chem. 271 (1996) 30858–30863.

[12] M. Asakura, M. Kitakaze, S. Takashima, Y. Liao, F. Ishikura, T. Yoshinaka, H. Ohmoto, K. Node, K. Yoshino, H. Ishiguro, H. Asanuma, S. Sanada, Y. Matsumura, H. Takeda, S. Beppu, M. Tada, M. Hori, S. Higashiyama, Cardiac hypertrophy is inhibited by antagonism of ADAM12 processing of HB-EGF: metalloproteinase inhibitors as a new therapy, Nat. Med. 8 (2002) 35–40.

[13] D. Nanba, S. Higashiyama, Dual intracellular signaling by proteolytic cleavage of membrane-anchored heparin-binding EGF-like growth factor, Cytokine Growth Factor Rev. 15 (2004) 13–19.

[14] K. Goishi, S. Higashiyama, M. Klagsbrun, N. Nakano, T. Umata, M. Ishikawa, E. Mekada, N. Taniguchi, Phorbol ester induces the rapid processing of cell surface heparin-binding EGF-like growth factor: conversion from juxtacrine to paracrine growth factor activity, Mol. Biol. Cell 6 (1995) 967–980.

[15] D. Nanba, A. Mammoto, K. Hashimoto, S. Higashiyama, Proteolytic release of the carboxy-terminal fragment of proHB-EGF causes nuclear export of PLZF, J. Cell Biol. 163 (2003) 489–502.

[16] J. Bao, D. Wolpowiz, L.W. Role, D.A. Talmage, Back signaling by the Nrg-1 intracellular domain, J. Cell Biol. 161 (2003) 1133–1141.

[17] S.M. Dethlefsen, G. Raab, M.A. Moses, R.M. Adam, M. Klagsburn, M.R. Freeman, Extracellular calcium influx stimulates metalloproteinase cleavage and secretion of heparin-binding EGF-like growth factor independently of protein kinase C, J. Cell. Biochem. 69 (1998) 143–153.

[18] M. Vecchi, L.A. Rudolph-Owen, C.L. Brown, P.J. Dempsey, G. Carpenter, Tyrosine phosphorylation and proteolysis. Pervanadate-induced, metalloprotease-dependent cleavage of the ErbB-4 receptor and amphiregulin, J. Biol. Chem. 273 (1998) 20589–20595.

Prolonged Endoplasmic Reticulum Stress in Hypertrophic and Failing Heart After Aortic Constriction

Possible Contribution of Endoplasmic Reticulum Stress to Cardiac Myocyte Apoptosis

Ken-ichiro Okada, MD*; Tetsuo Minamino, MD, PhD*; Yoshitane Tsukamoto, MD, PhD*;
Yulin Liao, MD; Osamu Tsukamoto, MD; Seiji Takashima, MD, PhD; Akio Hirata, MD;
Masashi Fujita, MD; Yoko Nagamachi, BS; Takeshi Nakatani, MD, PhD; Chikao Yutani, MD, PhD;
Kentaro Ozawa, MD, PhD; Satoshi Ogawa, MD, PhD; Hitonobu Tomoike, MD, PhD;
Masatsugu Hori, MD, PhD; Masafumi Kitakaze, MD, PhD

Background—The endoplasmic reticulum (ER) is recognized as an organelle that participates in folding secretory and membrane proteins. The ER responds to stress by upregulating ER chaperones, but prolonged and/or excess ER stress leads to apoptosis. However, the potential role of ER stress in pathophysiological hearts remains unclear.

Methods and Results—Mice were subjected to transverse aortic constriction (TAC) or sham operation. Echocardiographic analysis demonstrated that mice 1 and 4 weeks after TAC had cardiac hypertrophy and failure, respectively. Cardiac expression of ER chaperones was significantly increased 1 and 4 weeks after TAC, indicating that pressure overload by TAC induced prolonged ER stress. In addition, the number of terminal deoxynucleotidyl transferase–mediated dUTP nick-end labeling (TUNEL)–positive cells increased, and caspase-3 was cleaved in failing hearts. The antagonism of angiotensin II type 1 receptor prevented upregulation of ER chaperones and apoptosis in failing hearts. On the other hand, angiotensin II upregulated ER chaperones and induced apoptosis in cultured adult rat cardiac myocytes. We also investigated possible signaling pathways for ER-initiated apoptosis. The CHOP- (a transcription factor induced by ER stress), but not JNK- or caspase-12-, dependent pathway was activated in failing hearts by TAC. Pharmacological ER stress inducers upregulated ER chaperones and induced apoptosis in cultured cardiac myocytes. Finally, mRNA levels of ER chaperones were markedly increased in failing hearts of patients with elevated brain natriuretic peptide levels.

Conclusions—These findings suggest that pressure overload by TAC induces prolonged ER stress, which may contribute to cardiac myocyte apoptosis during progression from cardiac hypertrophy to failure. (***Circulation.*** 2004;110:705-712.)

Key Words: apoptosis ■ hypertrophy ■ heart failure ■ endoplasmic reticulum

The endoplasmic reticulum (ER) is recognized as an organelle that participates in the folding of secretory and membrane proteins.[1,2] Histological examination has demonstrated that the ER develops markedly in hypertrophic and failing hearts.[3,4] It has been reported that the synthesis of secretory proteins, such as atrial natriuretic peptide (ANP) and brain natriuretic peptide (BNP), is increased in hypertrophic and failing hearts.[5] As the acceleration of protein synthesis is prolonged, cells adapt to the increased protein synthesis load by the development of the ER, which involves coordinated expression of numerous genes encoding ER-resident proteins.[6-8] Thus, the development of the ER in hypertrophic and failing hearts may indicate the compensatory response to the elevated protein synthesis.

Another emerging function of the ER is to regulate apoptosis.[9,10] Various stimuli, such as ischemia, hypoxia, heat shock, gene mutation, and elevated protein synthesis, all of which can potentially cause ER dysfunction, are collectively known as ER stress.[1,2] In response to ER stress, there is marked upregulation of ER chaperones such as glucose-

A

B

C

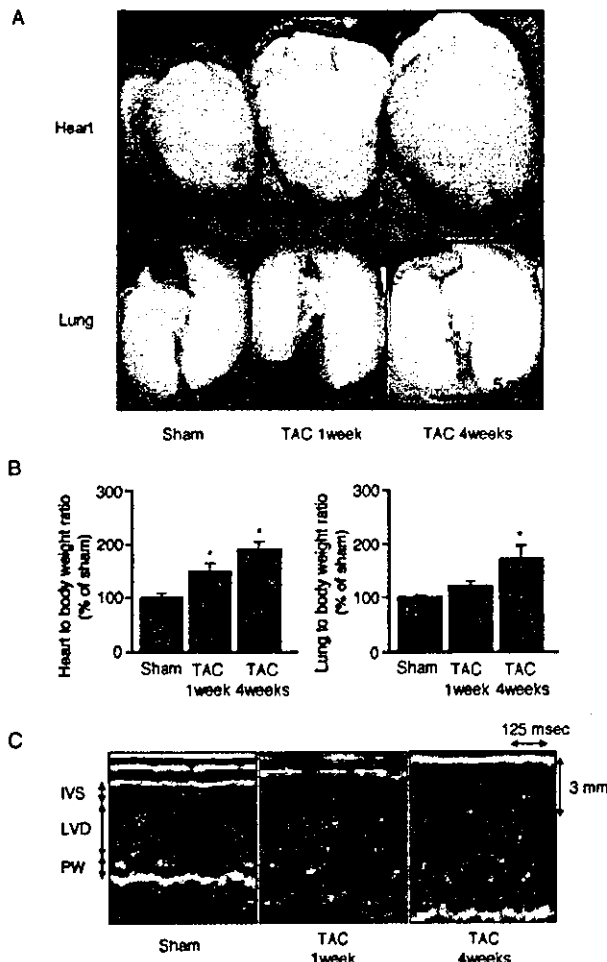**Figure 1.** Cardiac hypertrophy and failure induced by TAC in mice. A, Representative images of hearts and lungs. B, Heart and lung to body weight ratio. *$P<0.05$ vs sham operation. Each group consists of 3 to 5 mice. C, Representative echocardiograms in mouse hearts after TAC. IVS indicates interventricular septum; LVD, LV dimension; and PW, posterior wall.

regulated protein 94 kDa (GRP94), GRP78, and calreticulin.[1,10,11] When ER stress is excess and/or prolonged, however, the initiation of the apoptotic processes is promoted by transcriptional induction of C/EBP homologous protein (CHOP) or by the activation of c-JUN NH$_2$-terminal kinase (JNK)— and/or caspase-12–dependent pathways.[12] Accumulating evidence demonstrates that apoptosis initiated by the

ER is involved in the pathogenesis of neurodegenerative diseases and diabetes mellitus.[1,2,12,13] Interestingly, apoptosis is also the key contributor to cell loss in the setting of heart failure.[14,15] Because the development of the ER[3,4] and elevated protein synthesis in hearts[16] suggest that ER stress is induced in hypertrophic and failing hearts, we hypothesized that ER stress may contribute to cardiac myocyte apoptosis observed during progression from cardiac hypertrophy to failure. To test this hypothesis, we examined the potential role of ER stress–induced apoptosis in experimental models and failing human hearts. Furthermore, because the renin–angiotensin system plays an important role in the development of hypertrophic and failing hearts and angiotensin II increases protein synthesis that may potentially cause ER stress,[17] we also examined the role of angiotensin II in the induction of ER stress in pathophysiological hearts and cultured cardiac myocytes.

Methods

Antibodies and Reagents

Tunicamycin, thapsigargin, and angiotensin II were purchased from Sigma. Antibodies for GRP78, GRP94, calreticulin, and KDEL (Lys-Asp-Glu-Leu), which recognizes both GRP78 and GRP94, were purchased from StressGen. Antibodies for CHOP and actin were obtained from Santa Cruz Biotechnology. Antibodies for phospho-SAPK/JNK, SAPK/JNK, and cleaved caspase-3 were obtained from Cell Signaling Technology. The antibody for caspase-12 was obtained from BioVision. CS-866, an angiotensin II type 1 receptor blocker, and RNH-6270, an active metabolite of CS-866, were provided from Sankyo Co Ltd.[18]

Preparation of Rat Cardiac Myocytes

Primary cultures of neonatal (aged 2 to 3 days) and adult (aged 7 weeks; male) cardiac myocytes were prepared with the use of Wistar-Kyoto rats as described previously.[19,20] All procedures were performed in accordance with the guiding principles of Osaka University School of Medicine with regard to animal care and the *Position of the American Heart Association on Research Animal Use.*

Immunoblotting

Immunoblotting was performed as described previously,[20] and immunoreactive bands were quantified by densitometry (Molecular Dynamics).

Preparation of Human Heart Samples

Under the protocol approved by the institutional review board of the National Cardiovascular Center (No. 14-18), samples of human cardiac tissue were obtained. Tissue samples for RNA extraction were frozen at $-80°C$ until use, whereas the specimens for immunohistochemistry were fixed and embedded in paraffin.

Echocardiographic Data

	Sham (n=7)	TAC, 1 Week (n=9)	TAC, 4 Weeks (n=10)
Interventricular septum, mm	0.52±0.01	0.81±0.02*	0.99±0.01*
Posterior wall, mm	0.53±0.01	0.75±0.01*	0.97±0.02*
Left ventricular end-diastolic dimension, mm	2.85±0.05	2.84±0.09	3.15±0.06*
Left ventricular end-systolic dimension, mm	1.52±0.07	1.50±0.05	1.89±0.04*
Fractional shortening, %	46.4±1.8	47.2±1.0	40.0±1.0*

Values are mean±SEM. Fractional shortening was calculated as (left ventricular end-diastolic dimension − left ventricular end-systolic dimension) ÷ left ventricular end-diastolic dimension.
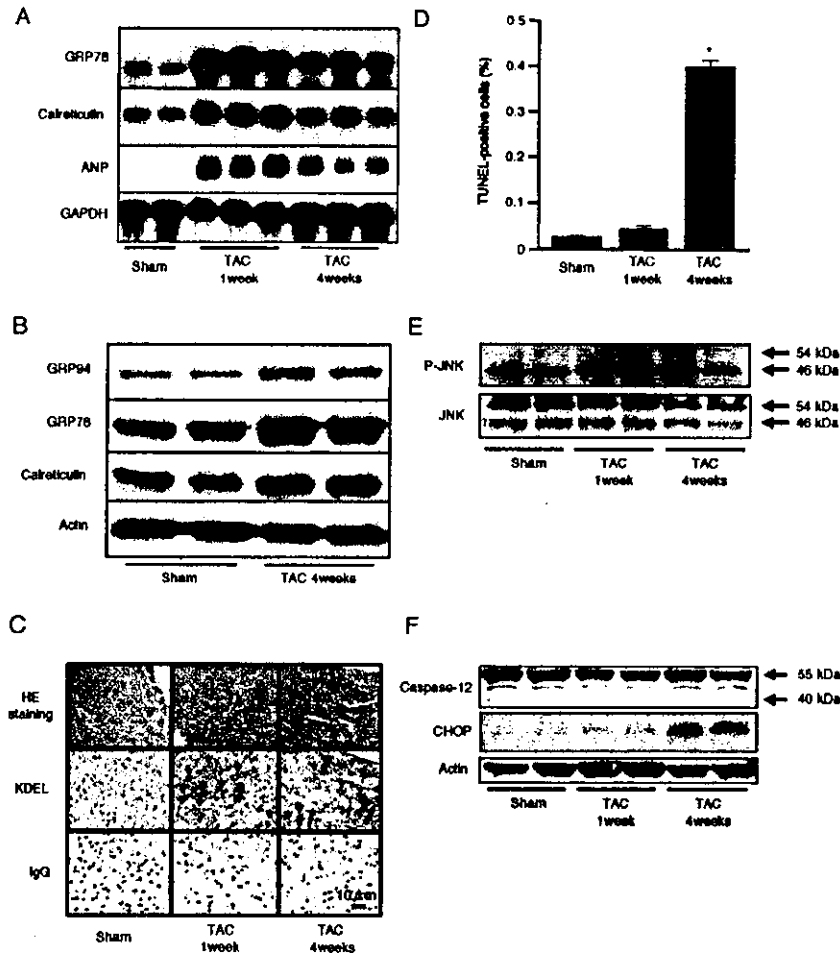*$P<0.05$ vs sham operation.

Figure 2. Upregulation of ER chaperones in hypertrophic and failing mouse hearts. A, mRNA levels of ER chaperones in the heart. B, Protein levels of ER chaperones in the failing heart. C, Hematoxylin-eosin (HE) (top), KDEL (middle), and IgG (bottom) staining of mouse hearts. D, Quantitative analysis of TUNEL-positive cardiac myocytes in mouse hearts. E, F, Phosphorylation of JNK, cleavage of caspase-12, and induction of CHOP in mouse heart. *$P<0.05$ vs sham operation.

Northern Blot Analysis

Northern blotting was performed as described previously.[21] To synthesize specific probes for Northern blotting, we used the following sense and antisense primers: 5'-GCCACGGGATGGTTCCTTGCC-3' and 5'-GCGGATCCAGGTCGACGCCGGCCA-3' for GRP78 (398 bp); 5'-CTGTGGGGGCGGCTATGTGA-3' and 5'-CACCCCAAATCC-GAACCAGC-3' for calreticulin (1069 bp); 5'-GCATTCCA-GCTCCTAGGTCAGA-3' and 5'-GGCTCCAATCCTGTCCATCC-3' for ANP (375 bp); 5'-AGTCCCTCCAGAGACATG-3' and 5'-CTTGTGGAATCAGAAGCA-3' for BNP (462 bp); and 5'-TCACCATCTTCCAGGAGCGA-3' and 5'-TCCTTGGAGGCC-ATGTGGGC-3' for GAPDH (784 bp), respectively. As the normal controls, we used total human heart RNA purchased from BD Bioscience and BioChain.

Immunohistochemical Analysis

Immunohistochemistry was performed as described previously.[22]

TAC Model

C57BL/6 mice (aged 8 weeks; male) were subjected to TAC or sham operation as described previously.[23] Echocardiography was performed on the mice as described previously.[23] CS-866 (1 mg/kg per day) was administered by gavage 1 day after TAC operation.

Apoptotic Cell Assay

Terminal deoxynucleotidyl transferase–mediated dUTP nick-end labeling (TUNEL) reaction was performed with the use of ApopTag apoptosis detection kits (Intergen Company). DNA ladder was performed as described previously.[24] Double staining for TUNEL and desmin (DakoCytomation) was performed in the left ventricular

(LV) free wall of mice. Neonatal rat cardiac myocytes were treated with tunicamycin (0.1 μg/mL) or thapsigargin (0.1 μmol/L) for 48 hours and stained for TUNEL and sarcomeric myosin heavy chain (MF-20) (Hybridoma Bank, University of Iowa). Numbers of TUNEL-positive cells counted in desmin-positive cells (n=5000) and in MF-20–positive cells (n=500) are expressed as percentages.

MTT Assay

Cardiac myocytes were treated with tunicamycin or thapsigargin for 48 hours. Cell viability was assessed by MTT assay according to the manufacturer's instructions (Cell Counting Kit 8). The relative number of viable cells was determined by estimating the value for untreated cells as 100%.

Statistical Analysis

Data are expressed as mean±SEM. Results were compared by 1-way ANOVA followed by Bonferroni's test. Comparisons of categorical variables were generated by Fisher's exact test. $P<0.05$ was accepted as statistically significant.

Results

Cardiac Hypertrophy and Failure in Mice After TAC

One week after the onset of TAC, cardiac enlargement was detected without severe lung congestion (Figure 1A, 1B). In contrast, cardiac enlargement was more prominent along with marked lung congestion 4 weeks after TAC (Figure 1A, 1B). Echocardiographic analysis also revealed LV dilatation and
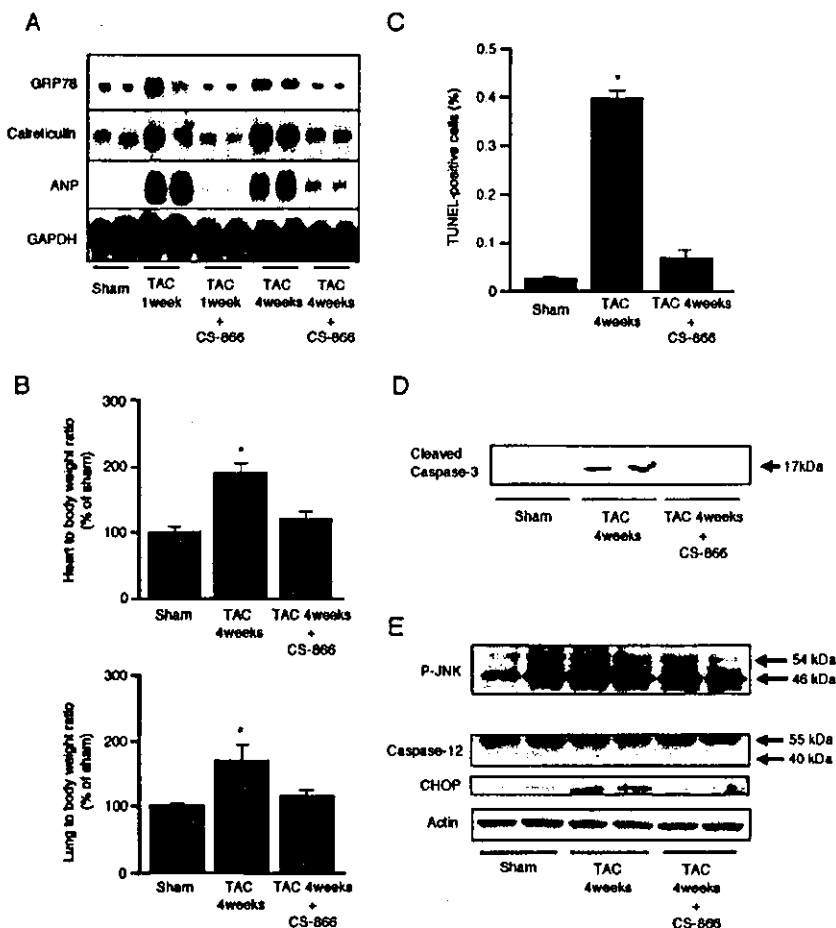
Figure 3. Prevention of ER chaperone expression by CS-866 in mouse hearts after TAC. A, mRNA levels of ER chaperones and ANP in mouse hearts after TAC. Effects of CS-866 on the development of cardiac hypertrophy (B), number of TUNEL-positive cells (C), caspase-3 cleavage (D), and ER-mediated apoptotic signals (E) in failing mouse hearts are shown. *$P<0.05$ vs sham operation.

LV systolic dysfunction 4 weeks, but not 1 week, after TAC. Increases in LV wall thickness were found 1 week after TAC and thereafter (Table, Figure 1C). These findings indicate that the mice 1 and 4 weeks after surgery corresponded to models of cardiac hypertrophy and failure, respectively.

Upregulation of ER Chaperones in Hypertrophic and Failing Mouse Hearts

mRNA levels of ER chaperones including GRP78 and calreticulin and of ANP were increased by TAC (Figure 2A). Consistent with mRNA levels, protein levels of ER chaperones were increased in hearts after TAC (Figure 2B). Moreover, immunohistochemical analysis revealed that the number of KDEL-positive cells was increased in the hearts of the mice after TAC (Figure 2C). Furthermore, the number of TUNEL-positive cells was increased in the heart 4 weeks after TAC (Figure 2D). Next, we checked involvement of signaling pathways of ER-initiated apoptosis in the hearts after TAC. CHOP was markedly induced 4 weeks after TAC, which coincided with the timing of the appearance of apoptosis (Figure 2E). The caspase-12 cleavage or JNK phosphorylation was not observed in hearts after TAC (Figure 2E, 2F).

Prevention of ER Chaperone Expression by Antagonism of Angiotensin II Type 1 Receptor in Mouse Hearts After TAC

The administration of CS-866 markedly attenuated the induction of both ER chaperones and ANP (Figure 3A). Further-

more, this angiotensin II type 1 receptor blocker prevented the development of cardiac hypertrophy and failure (Figure 3B), decreased the number of TUNEL-positive cells (Figure 3C), and attenuated the cleavage of caspase-3 in the failing hearts (Figure 3D). CS-866 attenuated CHOP induction but did not affect phosphorylation of JNK or the cleavage of caspase-12 in the failing hearts (Figure 3E).

Upregulation of ER Chaperones and Apoptosis by Angiotensin II in Adult Rat Cardiac Myocytes

Using adult rat cardiac myocytes, we studied the effects of angiotensin II on the expression of ER chaperones and apoptosis (Figure 4A). Treatment of adult rat cardiac myocytes with angiotensin II (10^{-9} mol/L) for 24 hours induced cardiac myocyte apoptosis along with the inductions of ER chaperones and CHOP, either of which was inhibited by RNH-6270 (10^{-7} mol/L) (Figure 4B). Angiotensin II also increased protein synthesis evaluated by incorporation of [^{3}H]leucine, which was prevented by RNH-6270 (data not shown). Quantitative analysis revealed that angiotensin II increased KDEL-positive cells compared with no treatment ($5.0\pm0.1\%$ versus $16.0\pm1.1\%$; $P<0.05$; n=6000 each). The prevalence of TUNEL-positive cells in KDEL-positive ones was significantly higher than that in KDEL-negative ones ($P<0.05$, Fisher's exact test) (Figure 4B, 4C), indicating the association between ER stress and cardiac apoptosis. Furthermore, we could not find any KDEL-negative cells among
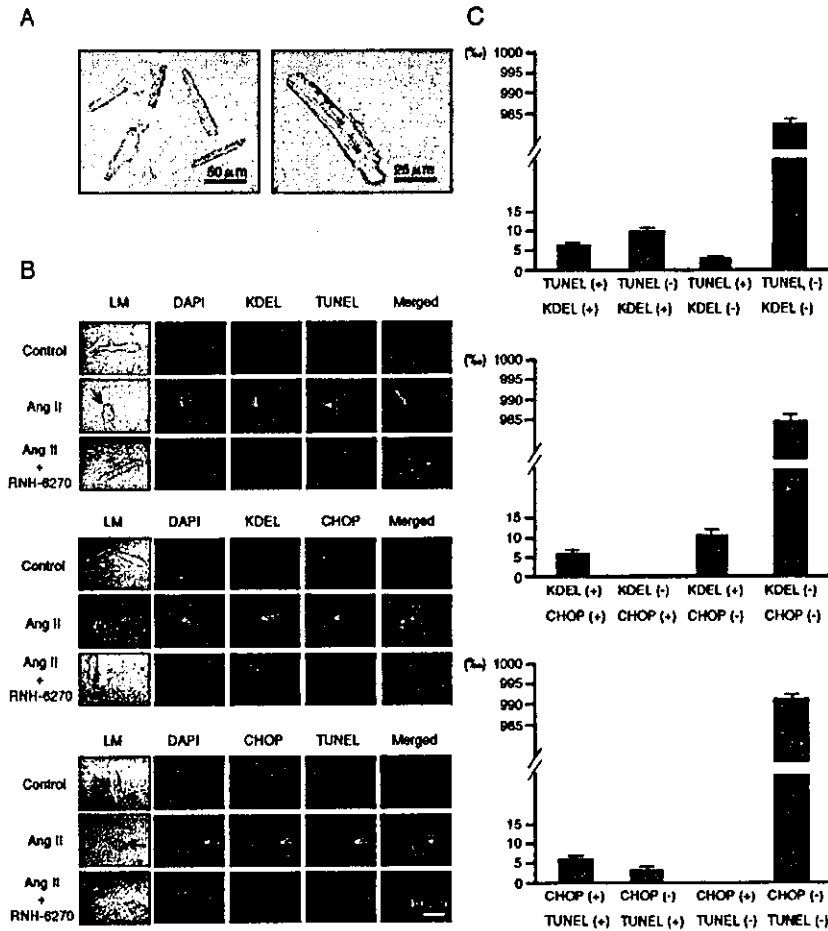
A

C

B

Figure 4. Upregulation of ER chaperones and apoptosis by angiotensin II in adult rat cardiac myocytes. A, Preparation of adult rat cardiac myocytes. B, CHOP, KDEL, and TUNEL staining in adult rat cardiac myocytes. C, Quantitative analysis of immunohistochemical staining after treatment with angiotensin II.

CHOP-positive ones, suggesting that CHOP specifically mediated ER-initiated signaling (Figure 4C). Importantly, there was a high prevalence of CHOP-positive cells among TUNEL-positive cells (69.7%) ($P<0.05$, Fisher's exact test), suggesting that CHOP-mediated signaling contributes to angiotensin II–induced cardiac apoptosis. RNH-6270 attenuated the upregulation of ER chaperones, induction of CHOP, or cardiac myocyte apoptosis (data not shown).

Apoptosis of Cultured Cardiac Myocytes Induced by Pharmacological Agents That Impair ER Function

Tunicamycin or thapsigargin, either of which impairs ER function,[1,9] increased protein levels of ER chaperones in cultured cardiac myocytes (Figure 5A). Treatment of cardiac myocytes with tunicamycin or thapsigargin caused a decrease of cell viability (Figure 5B) and an increase of TUNEL-positive cells in a dose-dependent manner (Figure 5C, 5D). Pharmacological ER stress inducers caused DNA fragmentation and the cleavage of caspase-3 (Figure 5E and 5F), and they induced CHOP expression, caspase-12 cleavage, and JNK phosphorylation in cultured cardiac myocytes (data not shown). Immunohistochemical analysis revealed that tunicamycin increased KDEL-positive cells compared with no treatment (31.6% versus 73.5%; $P<0.05$; n=500 each). The prevalence of TUNEL-positive cells in KDEL-positive ones

was significantly higher than that in KDEL-negative ones ($P<0.05$, Fisher's exact test) (Figure 5G and 5H), suggesting the association between ER stress and cardiac myocyte apoptosis.

Expression of ER Chaperones in Failing Human Hearts

In hematoxylin-eosin staining of cardiac tissue from patients with dilated cardiomyopathy, vacuolation was prominent, as previously reported.[3,4] Immunohistochemical analysis revealed that ER chaperones, including GRP78/GRP94 and calreticulin, were induced in the hearts of 2 patients with dilated cardiomyopathy (Figure 6A, d through f and g through i) but not in the hearts of control subjects (Figure 6A, a through c). These changes were also found in adriamycin-induced cardiomyopathy, in which the development of the ER was reported previously[3] (Figure 6A, j through l). We confirmed that areas in which ER chaperones were induced corresponded to vacuolation areas in hematoxylin-eosin staining (Figure 6A). We also examined the levels of mRNA for ER chaperones in the hearts of 2 control subjects (Figure 6B, lanes 1, 2) and 8 patients with dilated cardiomyopathy (Figure 6B, lanes 3 through 10). Consistent with the clinical diagnosis, mRNA levels of ANP and BNP were increased in the hearts of all 8 patients with dilated cardiomyopathy (lanes 3 through 10) but not in the hearts of control subjects (Figure
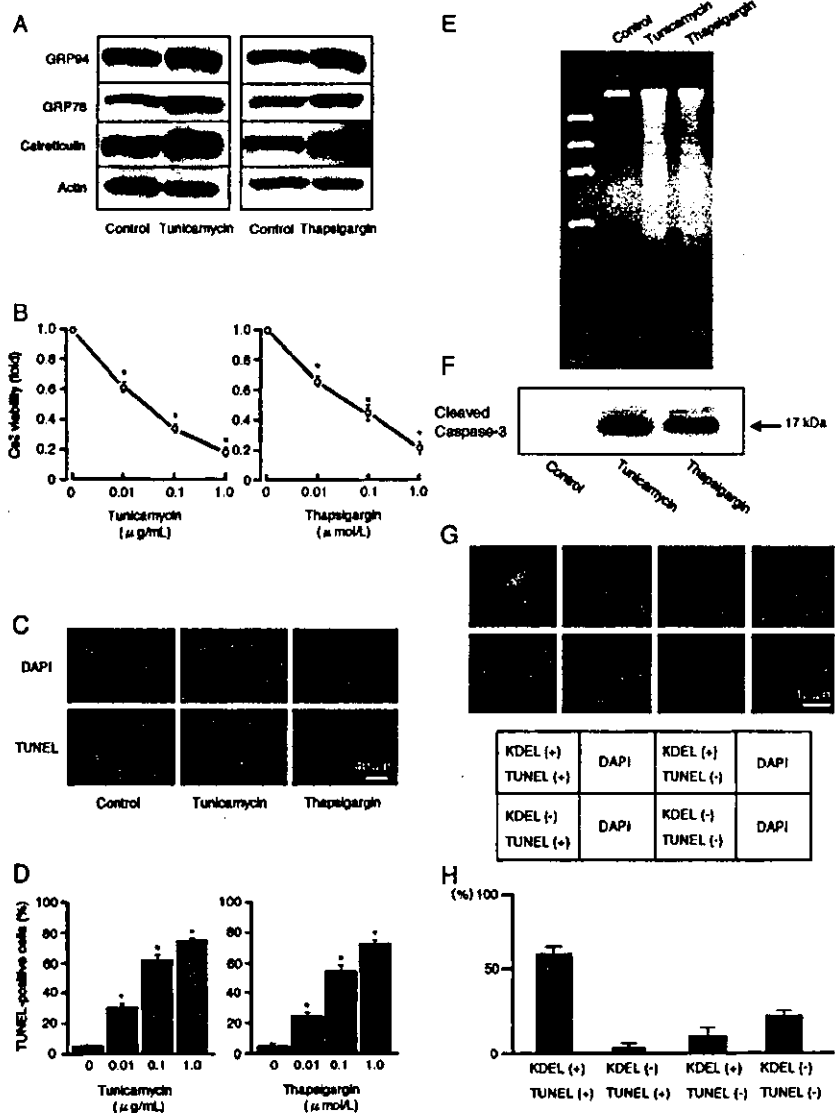
Figure 5. Induction of cardiac myocyte apoptosis by pharmacological ER stress inducers. A, Effects of tunicamycin (0.1 μg/mL) or thapsigargin (0.1 μmol/L) on protein levels of ER chaperones. B, Dose effects of tunicamycin or thapsigargin on cardiac myocyte viability. C, TUNEL staining of cardiac myocytes. D, Quantitative analysis of TUNEL-positive cardiac myocytes after treatment with tunicamycin or thapsigargin for 48 hours. *$P<0.05$ vs no treatment. DNA ladder (E) and cleavage of caspase-3 (F) in cardiac myocytes. G, Representative immunohistochemical pictures of cultured cardiac myocytes stained with KDEL and TUNEL stainings after tunicamycin. H, Quantitative analysis of TUNEL- or KDEL-positive cardiac myocytes treated with tunicamycin.

6B, lanes 1, 2). In 7 of the 8 patients with dilated cardiomyopathy (lanes 3 through 10), expression of both GRP78 and calreticulin was also markedly induced compared with the control subjects (Figure 6B).

Discussion

The ER is one of the largest cell organelles, and the ER lumen and internal spaces constitute >10% of the entire cell volume.[25] The functional and genomic analyses have revealed that the genes upregulated by ER stress account for 6% of the yeast genome.[26] These findings indicate that the ER is a highly dynamic organelle and plays essential roles in cell viability. The ER participates in folding of secretory and membrane proteins.[1,2] When the ER is overloaded to deal with the enhanced synthesis of secretory proteins, molecular compensatory mechanisms will operate (1) upregulation of ER chaperones, (2) reduced translation that decreases the load of new protein synthesis, and (3) degradation of proteins misfolded in the ER.[27] In the present study, we evaluated the upregulation of ER

chaperones as markers of ER stress. In mice with hypertrophic and failing hearts induced by TAC, we confirmed that ER chaperones were markedly induced. These findings suggest that pressure overload by TAC induces prolonged ER stress in the heart. The ER in the heart contains a high density of Ca^{2+}-ATPase and is often referred to as the sarcoplasmic reticulum.[28]

We demonstrated that CS-866, an angiotensin II type 1 receptor blocker, attenuated the upregulation of ER chaperones, the development of cardiac hypertrophy and failure, and cardiac myocyte apoptosis in TAC hearts. Furthermore, treatment of adult cardiac myocytes with angiotensin II induced ER chaperones as well as protein synthesis, either of which was prevented by RNII-6270. These findings suggest that cardiac ER stress is induced via an angiotensin II type 1 receptor-dependent pathway. Although it is likely that one of the potential mechanisms by which angiotensin II induced ER stress is enhanced protein synthesis, further investigation about the intracellular signaling pathway by which angiotensin II induces ER stress will be needed.
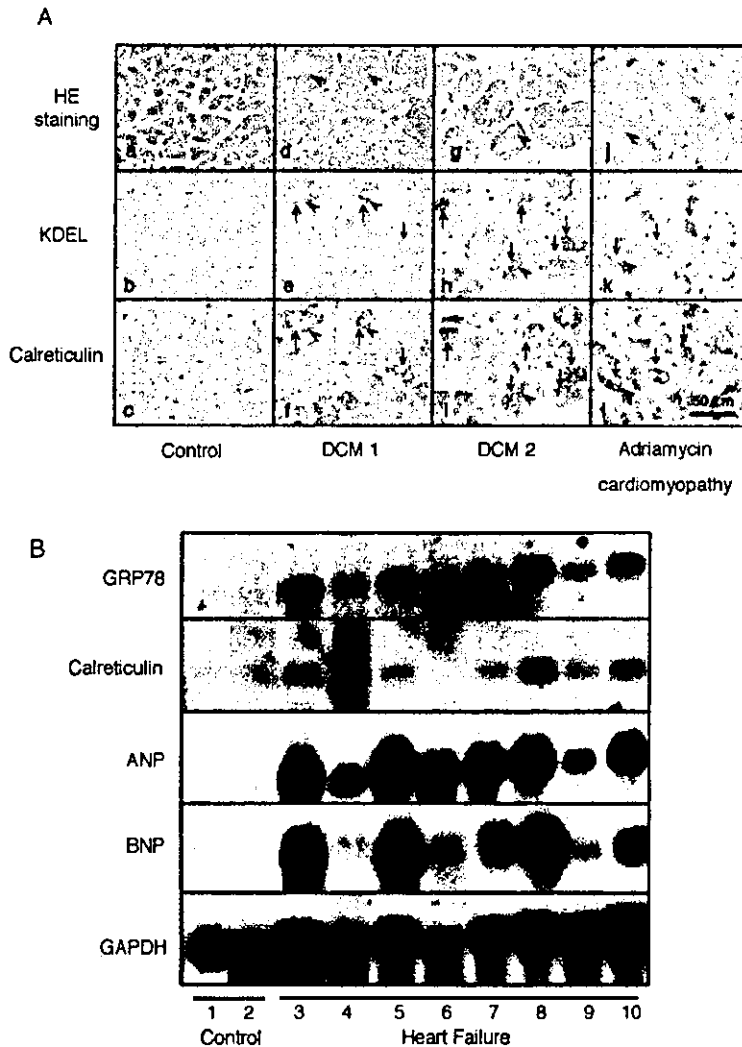
A

Figure 6. Expression of ER chaperones in failing human hearts. A, Immunohistochemical analysis of ER chaperones in human hearts. Panels a through c show tissue samples from an autopsied patient with normal cardiac function. Panels d through f show endomyocardial biopsy specimens from a patient with dilated cardiomyopathy (DCM). Panels g through i show a surgical specimen from a patient with dilated cardiomyopathy on mechanical ventricular support. Panels j through l show an endomyocardial biopsy specimen from a patient with adriamycin cardiomyopathy. Top, middle, and bottom panels show hematoxylin-eosin (HE), KDEL, and calreticulin stainings, respectively. Arrows in the figures indicate perinuclear and cytoplasmic reticular membrane structures stained with both anti-KDEL antibody and anti-calreticulin antibody. Arrowheads indicate that vacuolation areas found in hematoxylin-eosin staining corresponded to areas in which ER chaperones were induced. B, mRNA levels of GRP78 and calreticulin in human hearts. Lanes 1 and 2 show normal human heart specimens obtained from Clontech and BioChain, respectively. Lanes 3 through 6 are LV specimens from autopsy of patients with dilated cardiomyopathy, and lanes 7 through 10 are LV specimens from the native hearts of heart transplantation recipients.

Recent studies have demonstrated the occurrence of organelle-specific initiation of cell death.[10] Upregulation of ER chaperones was found in the heart from 1 week after TAC, suggesting the possibility that the ER initiates cardiac myocyte apoptosis. However, TUNEL-positive cells were not seen at 1 week after TAC and only became apparent at 4 weeks after TAC. If apoptosis in failing hearts was due to ER stress, time courses of the onsets of ER stress and cardiac apoptosis/dysfunction were inconsistent. This discrepancy between ER stress and the delayed appearance of pathological changes is also found in PKR-like ER kinase (PERK)-deficient mice that cannot reduce the initiation of translation in response to ER stress.[29] Prolonged ER stress is needed to impair the β-cell function that precedes metabolic decompensation in PERK-deficient mice. In the clinical setting, presenilin-1 gene mutation linked to early-onset familial Alzheimer's disease is known to downregulate the unfolded protein response and increase vulnerability to ER stress.[30] Usually, dementia due to presenilin-1 gene mutation appears in the 40s. These findings suggest that prolonged ER stress would be essential to cause overt pathological conditions.

ER stress induces apoptosis through CHOP-, JNK-, and caspase-12– dependent signaling pathways.[12] CHOP is in-duced at the transcription level mainly when the ER is stressed.[12,31] The overexpression of CHOP leads to growth arrest and apoptosis.[1,12,32] Thus, the induction of CHOP indicates that the ER-initiated apoptosis is promoted. Caspase-12 is located on the ER membrane and is activated only by ER stress.[10,12,33] JNK belongs to the stress-activated protein kinases and has been shown to induce apoptosis in response to ER stress.[10,12] We demonstrated that the number of TUNEL-positive cardiac myocytes was significantly increased in mouse hearts 4 weeks after TAC, and CHOP, but not JNK or caspase-12, was simultaneously induced. Because CHOP is a transcription factor that specifically mediates ER-initiated apoptosis, the induction of CHOP in failing hearts after TAC indicates that ER-initiated apoptosis is promoted under these conditions. However, because these 3 signaling pathways were activated in response to ER stress inducers in cultured rat cardiac myocytes, we cannot exclude the possibility that signaling pathways other than CHOP are activated at different timings.

We used tunicamycin or thapsigargin as a pharmacological ER stress inducer.[1,10,13] Thapsigargin is the ER Ca^{2+}-ATPase inhibitor that leads to ER stress.[13,33] On the other hand,

tunicamycin is a specific inhibitor of *N*-glycosylation, a process that is observed only in the ER, indicating that this agent is a highly specific ER stress inducer.[13,33] Immunohistochemical analysis revealed the association between KDEL-positive cells and apoptotic cells when neonatal rat cardiac myocytes were treated with tunicamycin, supporting the idea that ER stress can initiate apoptotic signaling in cardiac myocytes. The difference in number of KDEL-positive cells in neonatal and adult cardiac myocytes is probably due to the differences in protein synthetic capacity and/or the presence of fetal calf serum in cultured medium.

The heart could become a neuroendocrine organ in the setting of chronic heart failure.[5] We found that both the ER expansion and the upregulation of ER chaperones were found in patients with heart failure. These changes suggestive of ER stress in human chronic heart failure may be attributed to prolonged elevation of protein synthesis such as ANP and BNP. These findings suggest that ER-initiated apoptosis due to prolonged ER stress in failing human hearts may also be involved in the development and progression of clinical heart failure.[14,15]

In conclusion, to our knowledge, the present study is the first demonstration of ER stress in hypertrophic and failing hearts under experimental and clinical conditions. Our findings suggest that ER-initiated apoptosis may contribute to cardiac myocyte apoptosis in failing hearts.

Acknowledgments

References

1. Kaufman RJ. Stress signaling from the lumen of the endoplasmic reticulum: coordination of gene transcriptional and translational controls. *Genes Dev.* 1999;13:1211–1233.
2. Ron D. Translational control in the endoplasmic reticulum stress response. *J Clin Invest.* 2002;110:1383–1388.
3. Ferrans VJ, Butany JW. Ultrastructural pathology of the heart. In: Trump BF, Jones RT, eds. *Diagnostic Electron Microscopy*. Vol 4. New York, NY: John Wiley & Sons; 1983:319–473.
4. Maron BJ, Ferrans VJ, Roberts WC. Ultrastructural features of degenerated cardiac muscle cells in patients with cardiac hypertrophy. *Am J Pathol.* 1975;79:387–434.
5. Cameron VA, Ellmers LJ. Minireview: natriuretic peptides during development of the fetal heart and circulation. *Endocrinology.* 2003;144:2191–2194.
6. Kaufman RJ, Scheuner D, Schroder M, et al. The unfolded protein response in nutrient sensing and differentiation. *Nat Rev Mol Cell Biol.* 2002;3:411–421.
7. Dorner AJ, Wasley LC, Kaufman RJ. Increased synthesis of secreted proteins induces expression of glucose-regulated proteins in butyrate-treated Chinese hamster ovary cells. *J Biol Chem.* 1989;264:20602–20607.
8. Pahl HL, Baeuerle PA. The ER-overload response: activation of NF-kappa B. *Trends Biochem Sci.* 1997;22:63–67.
9. Kaufman RJ. Orchestrating the unfolded protein response in health and disease. *J Clin Invest.* 2002;110:1389–1398.
10. Ferri KF, Kroemer G. Organelle-specific initiation of cell death pathways. *Nat Cell Biol.* 2001;3:E255–E263.
11. Patterson C, Cyr D. Welcome to the machine: a cardiologist's introduction to protein folding and degradation. *Circulation.* 2002;106:2741–2746.
12. Oyadomari S, Araki E, Mori M. Endoplasmic reticulum stress-mediated apoptosis in pancreatic beta-cells. *Apoptosis.* 2002;7:335–345.
13. Nishitoh H, Matsuzawa A, Tobiume K, et al. ASK1 is essential for endoplasmic reticulum stress-induced neuronal cell death triggered by expanded polyglutamine repeats. *Genes Dev.* 2002;16:1345–1355.
14. Chandrashekhar Y, Narula J. Death hath a thousand doors to let out life. *Circ Res.* 2003;92:710–714.
15. Wencker D, Chandra M, Nguyen K, et al. A mechanistic role for cardiac myocyte apoptosis in heart failure. *J Clin Invest.* 2003;111:1497–1504.
16. Siddiq T, Patel VB, Sherwood R, et al. In vivo protein synthetic rates of atrial, ventricular, and pulmonary tissue proteins in aortic constriction, Goldblatt, and bromoethylamine models of hypertension. *Exp Mol Pathol.* 2001;70:19–30.
17. Schunkert H, Sadoshima J, Cornelius T, et al. Angiotensin II–induced growth responses in isolated adult rat hearts: evidence for load-independent induction of cardiac protein synthesis by angiotensin II. *Circ Res.* 1995;76:489–497.
18. Koike H, Sada T, Mizuno M, et al. In vitro and in vivo pharmacology of olmesartan medoxomil, an angiotensin II type AT1 receptor antagonist. *J Hypertens Suppl.* 2001;19:S3–S14.
19. Maruyama R, Takemura G, Aoyama T, et al. Dynamic process of apoptosis in adult rat cardiomyocytes analyzed using 48-hour videomicroscopy and electron microscopy: beating and rate are associated with the apoptotic process. *Am J Pathol.* 2001;159:683–691.
20. Minamino T, Gaussin V, DeMayo FJ, et al. Inducible gene targeting in postnatal myocardium by cardiac-specific expression of a hormone-activated Cre fusion protein. *Circ Res.* 2001;88:587–592.
21. Tsukamoto Y, Kuwabara K, Hirota S, et al. 150-kD oxygen-regulated protein is expressed in human atherosclerotic plaques and allows mononuclear phagocytes to withstand cellular stress on exposure to hypoxia and modified low density lipoprotein. *J Clin Invest.* 1996;98:1930–1941.
22. Minamino T, Kitakaze M, Papst PJ, et al. Inhibition of nitric oxide synthesis induces coronary vascular remodeling and cardiac hypertrophy associated with the activation of p70 S6 kinase in rats. *Cardiovasc Drugs Ther.* 2000;14:533–542.
23. Liao Y, Ishikura F, Beppu S, et al. Echocardiographic assessment of LV hypertrophy and function in aortic-banded mice: necropsy validation. *Am J Physiol.* 2002;282:1703–1708.
24. Minamino T, Yujiri T, Papst PJ, et al. MEKK1 suppresses oxidative stress-induced apoptosis of embryonic stem cell-derived cardiac myocytes. *Proc Natl Acad Sci U S A.* 1999;96:15127–15132.
25. Travers KJ, Patil CK, Wodicka L, et al. Functional and genomic analyses reveal an essential coordination between the unfolded protein response and ER-associated degradation. *Cell.* 2000;101:249–258.
26. Martinez IM, Chrispeels MJ. Genomic analysis of the unfolded protein response in Arabidopsis shows its connection to important cellular processes. *Plant Cell.* 2003;15:561–576.
27. Mori K. Tripartite management of unfolded proteins in the endoplasmic reticulum. *Cell.* 2000;101:451–454.
28. Berridge MJ. The endoplasmic reticulum: a multifunctional signaling organelle. *Cell Calcium.* 2002;32:235–249.
29. Harding HP, Ron D. Endoplasmic reticulum stress and the development of diabetes: a review. *Diabetes.* 2002;51:S455–S461.
30. Imaizumi K, Miyoshi K, Katayama T, et al. The unfolded protein response and Alzheimer's disease. *Biochim Biophys Acta.* 2001;1536:85–96.
31. McCullough KD, Martindale JL, Klotz LO, et al. Gadd153 sensitizes cells to endoplasmic reticulum stress by down-regulating Bcl2 and perturbing the cellular redox state. *Mol Cell Biol.* 2001;21:1249–1259.
32. Wang XZ, Lawson B, Brewer JW, et al. Signals from the stressed endoplasmic reticulum induce the C/EBP-homologous protein (CHOP/GADD153). *Mol Cell Biol.* 1996;16:4273–4280.
33. Nakagawa T, Zhu H, Morishima N, et al. Caspase-12 mediates endoplasmic-reticulum-specific apoptosis and cytotoxicity by amyloid-beta. *Nature.* 2000;403:98–103.

HB-EGF Is a Potent Inducer of Tumor Growth and Angiogenesis

Pat P. Ongusaha,[1] Jennifer C. Kwak,[1] Andrew J. Zwible,[1] Salvador Macip,[2] Shigeki Higashiyama,[3] Naoyuki Taniguchi,[4] Li Fang,[5] and Sam W. Lee[1]

[1]Cancer Biology Program, Hematology and Oncology Division, Beth Israel Deaconess Medical Center and Harvard Medical School, Boston, Massachusetts; [2]Derald H. Ruttenberg Cancer Center, Mount Sinai School of Medicine, New York, New York; [3]Department of Medical Biochemistry, Ehime University School of Medicine, Ehime, Japan; [4]Department of Biochemistry, Osaka University Medical School, Osaka, Japan; and [5]Telik, Inc., Palo Alto, California

ABSTRACT

Heparin-binding epidermal growth factor-like growth factor (HB-EGF) has been shown to stimulate the growth of a variety of cells in an autocrine or paracrine manner. Although HB-EGF is widely expressed in tumors compared with normal tissue, its contribution to tumorigenicity is unknown. HB-EGF can be produced as a membrane-anchored form (pro-HB-EGF) and later processed to a soluble form (s-HB-EGF), although a significant amount of pro-HB-EGF remains uncleaved on the cell surface. To understand the roles of two forms of HB-EGF in promoting tumor growth, we have studied the effects of HB-EGF expression in the process of tumorigenesis using in vitro and in vivo systems. We demonstrate here that in EJ human bladder cancer cells containing a tetracycline-regulatable s-HB-EGF or pro-HB-EGF expression system, s-HB-EGF expression increased their transformed phenotypes, including growth rate, colony-forming ability, and activation of cyclin D1 promoter, as well as induction of vascular endothelial growth factor in vitro. Moreover, s-HB-EGF or wild-type HB-EGF induced the expression and activities of the metalloproteases, MMP-9 and MMP-3, leading to enhanced cell migration. In vivo studies also demonstrated that tumor cells expressing s-HB-EGF or wild-type HB-EGF significantly enhanced tumorigenic potential in athymic nude mice and exerted an angiogenic effect, increasing the density and size of tumor blood vessels. However, cells expressing solely pro-HB-EGF did not exhibit any significant tumorigenic potential. These findings establish s-HB-EGF as a potent inducer of tumor growth and angiogenesis and suggest that therapeutic intervention aimed at the inhibition of s-HB-EGF functions may be useful in cancer treatment.

INTRODUCTION

Heparin-binding epidermal growth factor-like growth factor (HB-EGF) is a heparin-binding member of the EGF family (1), which was initially identified in the conditional medium of human macrophages (2). It is a potent mitogen and chemotactic factor for fibroblasts and smooth muscle cells (3–5). As with other EGF family members, HB-EGF binds and activates EGF receptors 1 and 4 (1, 6, 7). Moreover, HB-EGF has been shown to stimulate the growth of a variety of cells in an autocrine or paracrine manner and to be involved in stromal proliferation (8). HB-EGF is initially synthesized as a transmembrane protein of 208 amino acids (1). Although the membrane-anchored form of HB-EGF (pro-HB-EGF) is cleaved on the cell surface to yield a soluble growth factor of 75–86 amino acids, a considerable amount of pro-HB-EGF remains uncleaved on the cell surface (1). Pro-HB-EGF is not merely a precursor of the soluble form; it is biologically active such that it forms complexes with both CD9 (9) and integrin $\alpha_3\beta_1$ (10) and transduces biological signals to neighboring cells in a nondiffusible manner (7). The transmembrane form of HB-EGF is a juxtacrine growth factor, which is immobilized on the surface of the cell and interacts with neighboring cells (1). It has also been shown

that the transmembrane HB-EGF synthesized by one type of cell can stimulate tyrosine phosphorylation of the EGF receptor in another type of cell in coculture (11). A recent study demonstrated that HB-EGF can bind to a novel 140-kDa receptor identified as N-arginine dibasic convertase, a metalloendopeptidase of the M16 family, and that binding to N-arginine dibasic convertase is highly specific for HB-EGF among EGF family members (12). Its specific binding modulates HB-EGF-induced cell migration via EGF receptor (12).

Several laboratories have described HB-EGF as being up-regulated in response to oncogenes and in oncogene-transformed cells (13, 14). In chicken embryo fibroblasts transfected with regulatable v-Jun, the expression of HB-EGF is greatly induced as v-Jun levels are increased (15), suggesting that HB-EGF plays an important part in mediating Jun-induced cell transformation. Furthermore, HB-EGF has been identified as an immediate-early response gene that can be activated by the Ras/Raf signaling pathway that mediates the autocrine activation of the c-Jun kinase in NIH3T3 cells (15). Phosphorylation of the transcription factor Ets-2 by activation of the Raf1/MAPK cascade regulates the induction of HB-EGF transcription in mouse fibroblasts (16). Additionally, in nontransformed human mammary epithelial cells, HB-EGF expression is induced by EGF and Ha-Ras overexpression (17), strongly implying that HB-EGF is a direct target of mitogen-activated protein kinase (MAPK). Our previous observations demonstrated that HB-EGF is induced in response to tumor suppressor p53, as well as DNA damage, and HB-EGF induction antagonizes apoptosis mediated by genotoxic stress through the activation of the Ras/Raf/MAPK cascade and the AKT pathway (18, 19), strongly suggesting a survival factor function for HB-EGF.

HB-EGF expression has been implicated in tumor progression because of its overexpression in many tumors, including hepatocarcinoma, colon, melanoma, myeloma, breast, prostate, and bladder tumors. It also has been implicated in increased proliferation and metastasis (20–27). Many tumor cells with HB-EGF overexpression are diphtheria toxin sensitive, suggesting that these cells accumulate the transmembrane form of HB-EGF. There is growing evidence of increased HB-EGF expression in tumors compared with normal tissue, e.g., pancreatic (28), liver (23, 29), esophageal (30), melanoma (20), bladder (31), and gastric tumors (32). Although HB-EGF is widely expressed in tumors and may be enhanced compared with normal tissue, its contribution to tumorigenicity is unknown. Moreover, it is not known whether the membrane-bound or the soluble form of HB-EGF contributes to tumorigenic processes.

In this study, we examined the biological effects of the two forms of HB-EGF on tumor growth and angiogenesis, using a tetracycline (tet)-regulated expression system in human EJ bladder carcinoma cells, which have a low basal level of HB-EGF. EJ cells expressing soluble form HB-EGF (s-HB-EGF) or wild-type HB-EGF (wt-HB-EGF) resulted in an increased growth rate, activation of the cyclin D promoter, colony-forming ability, and tumor growth in athymic nude mice. We also found that s-HB-EGF induced vascular endothelial growth factor (VEGF) expression, implicating an autocrine loop that may play a role in regulating these growth factors. Additionally, in response to s-HB-EGF, cells induced the expression and activities of the metalloproteases MMP-9 and MMP-3, leading to enhanced cell

5283

migration. In this study, we provide evidence of the biological activity of HB-EGF in tumorigenesis.

MATERIALS AND METHODS

Cell Culture and Transfection of Different Forms of HB-EGFs. Human bladder carcinoma cell line, EJ, expressing a tet activator, was transfected with wt-, s-, or pro-HB-EGF cDNA/pTet-puro and selected by continuous growth in puromycin (2 μg/ml) to isolate stable tet-regulated clones. Mutant constructs and expression of s-HB-EGF and pro-HB-EGF were described previously (33). Tet-regulatable EJ-HB-EGF cells were maintained in the presence of tet (1–2 μg/ml) in DMEM plus 10% FBS, 75 μg/ml hygromycin, and 2 μg/ml puromycin. Induction of each form of HB-EGF expression was achieved by washing the cells three times with PBS followed by addition of culture media without tet. For zymograms for MMP activity, cell culture media was concentrated 50-fold and loaded on to a 10% zymogram gel (Invitrogen, Carlsbad, CA). The MMP gel was renatured by incubating in renaturing buffer (Invitrogen) for 30 min at room temperature, and the MMP activity was examined by incubating in developing buffer for 24 h. MMP bands were visualized by staining with simply blue dye reagent (Invitrogen). The concentrated culture media were also immunoblotted with the mouse anti-MMP-9 and anti-MMP-3 monoclonal antibodies (Neomarkers, Fremont, CA). For cell proliferation assay, three different EJ-HB-EGF cell lines expressing wt-HB-EGF, s-HB-EGF, and pro-HB-EGF, respectively, were seeded on 6-well plates with or without tet at a density of 2 × 10⁴ cells/well. At days 2, 4, 6, and 8, cells were trypsinized, stained with trypan blue, and counted using a hemocytometer. Each data point was the average of three independent experiments.

Northern Blot and Western Blot Analyses. Total RNA was extracted, denatured, and electrophoresed through a 1% agarose-formaldehyde gel as described previously (19). Total protein extracts were immunoblotted with the respective antibodies. Tumors were dissected from the mice and snap frozen in liquid nitrogen. The tumors were then homogenized in lysis buffer containing 1% Triton X-100, 10 mM HEPES (pH 7.5), 130 mM NaCl, 5 mM EDTA, 10 mM $Na_4P_2O_7$, 100 mM NaF, 2 mM $NaVO_4$, 1 mM phenylmethylsulfonyl fluoride, 50 μg/ml leupeptin, and 50 μg/ml aprotinin. Twenty μg of proteins were loaded into each well and separated by a 4–12% NuPAGE gel (Invitrogen).

Transwell Migration Assay. The cells were plated at a cell density of 2 × 10⁵ cells in a 100-mm diameter dish. Each form of HB-EGF was induced by the removal of tet for 24 h, followed by serum starvation for another 24 h. Control cells were plated in similar conditions as HB-EGF-expressing cells, except that tet was added to suppress HB-EGF expression. Migration assays were performed using a chemotaxis chamber (Becton Dickinson and Co., Franklin Lakes, NJ) and transwell tissue culture plates (6.5 mm and 8-μm pore size). The bottom of the chamber was coated with either 10 μg/ml fibronectin, collagen I, or Matrigel (Sigma, St. Louis, MO). The uncoated sites were blocked with 10% BSA. One-hundred μl of 1 × 10⁵ cells/ml were introduced into each well and were allowed to migrate for 6 h. Cells were then fixed with methanol and stained with crystal violet. The migrated cells were quantified by counting the number of cells in five random ×200 fields. Each experiment was done in triplicates, and the experiment was repeated twice.

Wound-Healing Assay. HB-EGF was expressed for 24 h in the absence of tet, and control cells were seeded in the same fashion, except in the presence of tet. Cells were then seeded in a 6-well plate at a density of 1 × 10⁶ cells in the presence or absence of tet for 24 h. A wound was made using the tip of a
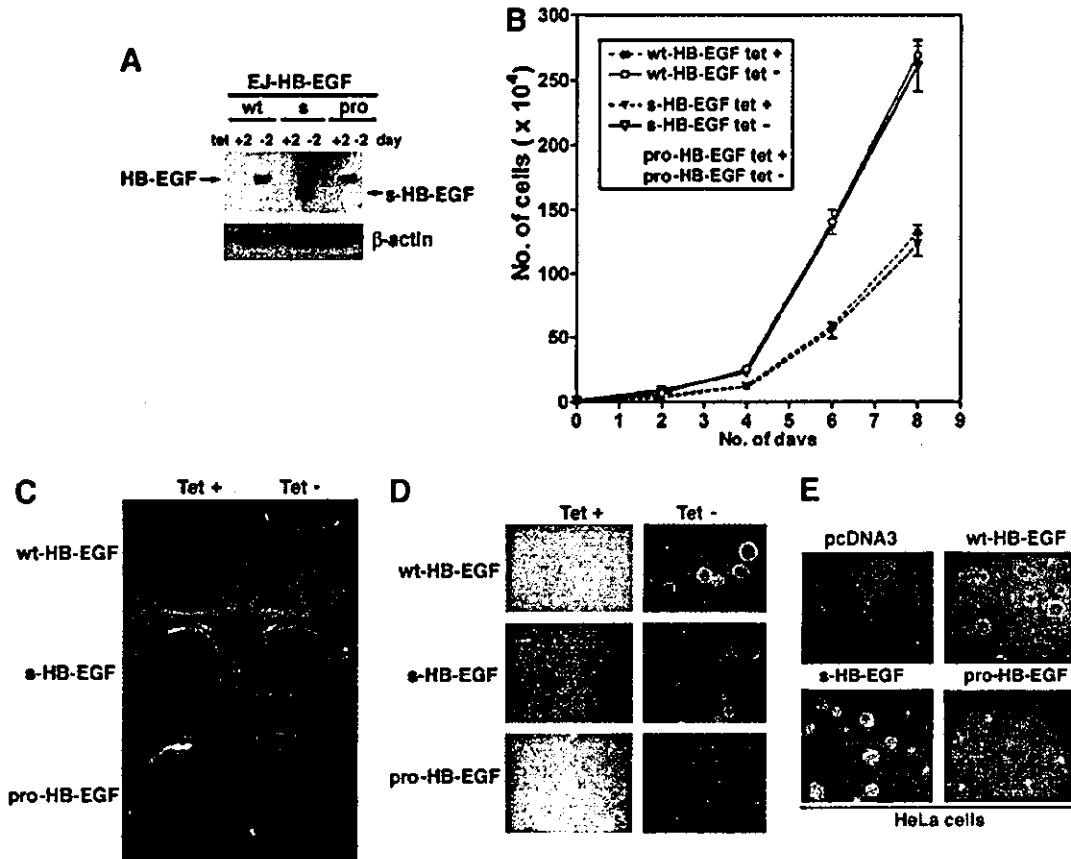

Fig. 1. Soluble heparin-binding epidermal growth factor-like growth factor (s-HB-EGF) enhances transformed phenotype in EJ human bladder carcinoma cells. *A*, inducible expression of three forms of HB-EGF in tetracycline (tet)-regulated expression system in EJ cells. Western blot analysis was performed in EJ-wt-HB-EGF, EJ-s-HB-EGF, or EJ-pro-HB-EGF cells grown in the absence or presence of tet (1 μg/ml). *B*, The growth rates of HB-EGF induced cells were measured in the absence or presence of tet. EJ cells expressing HB-EGF demonstrated significant increase in proliferation as compared with control cells. *C*, s-HB-EGF increases colony formation. *D*, tet-regulated s- or wild-type (wt)-HB-EGF expression enhances *in vitro*-transformed phenotype. HB-EGF expression enhanced anchorage-independent growth in soft agarose in tet-regulated EJ-s-HB-EGF and EJ-wt-HB-EGF cells but not in EJ-pro-HB-EGF cells. *E*, s-HB-EGF overexpression increases growth in soft agarose in HeLa cells. HeLa cells were transfected with constructs encoding wt-, s-, and membrane-anchored form (pro)-HB-EGF or the empty vector (pcDNA3). Cells were then harvested 36 h after transfection, equal cell numbers were seeded in 60-mm Petri dishes and grown under selection in G418 for 2 weeks.

5284